Wang, P., Prell, W.L., Blum, P., et al., 2000
Proceedings of the Ocean Drilling Program, Initial Reports Volume 184

3. EXPLANATORY NOTES[1]

Shipboard Scientific Party[2]

INTRODUCTION

In this chapter, we have assembled information that will help the reader understand the basis for our preliminary conclusions and also enable the interested investigator to select samples for further analysis. This information concerns only shipboard operations and analyses described in the site reports in the *Proceedings of the Ocean Drilling Program, Initial Reports,* volume. Methods used by various investigators for shore-based analyses of Leg 184 data will be described in the individual contributions published in the *Scientific Results* volume and in publications within various professional journals.

Drilling Operations

Two coring systems were used during Leg 184: the advanced hydraulic piston corer (APC) and the extended core barrel (XCB). These systems were applied to maximize core recovery in the sediments being cored. Each cored interval was ~9.5 m long, which is the length of a core barrel. In some cases, the drill string was "washed ahead" without recovering sediments in order to advance the drill bit to a target depth where core recovery needed to be resumed. Coring systems and their characteristics, such as drilling-related deformation, are summarized in the "Explanatory Notes" chapters of various previous *Initial Reports* volumes. The Leg 139 *Initial Reports* volume includes a particularly detailed description.

Drilled intervals are referred to in meters below rig floor (mbrf), which are measured from the kelly bushing on the rig floor to the bottom of the drill pipe, and meters below seafloor (mbsf), which are calculated. When sediments of substantial thickness cover the seafloor (as at all sites during Leg 184), the mbrf depth of the seafloor is determined with a mudline core, assuming 100% recovery for the cored interval in

[1]Examples of how to reference the whole or part of this volume.
[2]Shipboard Scientific Party addresses.

Ms 184IR-103

the first core. Water depth is calculated by subtracting the distance from the rig floor to sea level from the mudline measurement in mbrf. This water depth usually differs from precision depth recorder measurements by a few to several meters. The mbsf depths of core tops are determined by subtracting the seafloor depth from the core-top depth in mbrf. The core-top datums (in mbrf) from the driller are the ultimate depth reference for any further depth calculation procedures.

Curatorial Procedures and Sample Depth Calculations

Numbering of sites, holes, cores, and samples follows the standard Ocean Drilling Program (ODP) procedure. A full curatorial identifier for a sample consists of the leg, site, hole, core number, core type, section number, and interval in centimeters measured from the top of the core section. For example, a sample identification of 184-1143A-1H-1, 10–12 cm, would represent a sample removed from the interval between 10 and 12 cm below the top of Section 1, Core 1 (H designates that this core was taken with the APC system) of Hole 1143A during Leg 184.

Cored intervals are also referred to in "curatorial" mbsf. The mbsf of a sample is calculated by adding the depth of the sample below the section top and the lengths of all higher sections in the core to the core-top datum measured with the drill string. A sediment core from less than a few hundred mbsf may, in some cases, expand upon recovery (typically 10% in the upper 300 m), and its length may not necessarily match the drilled interval. In addition, a coring gap typically occurs between cores, as shown by composite depth construction (see **"Composite Section,"** p. 3). Thus, a discrepancy may exist between the drilling mbsf and the curatorial mbsf. For instance, the curatorial mbsf of a sample taken from the bottom of a core may be larger than that of a sample from the top of the subsequent core, where the latter corresponds to the drilled core-top datum.

During Leg 184, multiple APC holes (typically three) were cored at each site to construct a continuous composite section. This resulted in a meters composite depth (mcd) scale for each site that accommodates core expansion and drilling gaps through interhole correlation using closely spaced measurements of core physical properties (see **"Composite Section,"** p. 3).

Core Handling and Analysis

General core-handling procedures are described in previous *Initial Report* volumes and the *Shipboard Scientist's Handbook* and are only summarized here. As soon as cores arrived on deck, gas void and headspace samples were taken by means of a syringe (if applicable) for immediate analysis as part of the shipboard safety and pollution prevention program. Core-catcher samples were obtained for biostratigraphic analysis. When the core was cut in sections, whole-round samples were taken for shipboard interstitial water examinations. In addition, headspace gas samples were immediately extracted from the ends of cut sections and sealed in glass vials for light hydrocarbon analysis.

Before splitting, whole-round core sections were run through the multisensor track (MST), and thermal conductivity measurements were taken. The cores were then split into working and archive halves (from bottom to top), so investigators should be aware that older material could have been transported upward on the split face of each section. The working half of each core was described visually and by means of

smear slides and then sampled both for shipboard analysis—such as physical properties, carbonate, and bulk X-ray diffraction mineralogy—and for shore-based studies. Shipboard sampling was kept at a minimum during Leg 184 to allow for construction of a detailed sampling plan after the composite section was built. The archive-half sections were measured for color reflectance, run through the cryogenic magnetometer, and photographed with both black-and-white and color film. Close-up photographs were taken of particular features for illustrations in site summaries, as requested by individual scientists.

Both halves of the core were then put into labeled plastic tubes, sealed, and placed in cold storage space aboard the ship. At the end of the leg, the cores were transferred from the ship into refrigerated containers and shipped to the ODP Gulf Coast Core Repository in College Station, Texas.

COMPOSITE SECTION

Stratigraphers have demonstrated that a continuous sedimentary section is rarely recovered from a single ODP borehole because core-recovery gaps occur between successive APC and XCB cores, despite 100% or more nominal recovery (e.g., Prell, 1982; Ruddiman et al., 1987; Farrell and Janecek, 1991). Construction of a complete section, referred to as a splice, requires combining stratigraphic intervals from two or more holes cored at the same site. To minimize alignment of core-recovery gaps across holes, the depths below the seafloor from which cores are recovered is offset among the holes. This practice ensures that most intercore intervals missing within a given hole are recovered in at least one of the adjacent holes.

Before a splice can be constructed, the cores from the various holes must be stratigraphically correlated with each other. Such correlation enables development of a depth scale referred to as an mcd scale. This differs from the traditional (hole specific) depth scale, called the mbsf scale. The latter is based on the length that the drill string is advanced, core by core. In contrast, the mcd scale is built by assuming that the uppermost sediment (commonly referred to as the mudline) in the first core from a given hole is the sediment/water interface. This core becomes the "anchor" in the composite depth scale and is the only one with depths that are the same on both the mbsf and mcd scales. From this anchor, core-logging data are correlated among holes downsection. The depth offset (a constant) required to best align stratigraphic structure is added to the mbsf depth of all cores below. Our mcd and splice construction methodology follows that successfully employed during a number of legs (e.g., Hagelberg et al., 1992; Curry, Shackleton, Richter, et al., 1995; Jansen, Raymo, Blum, et al., 1996; Lyle, Koizumi, Richter, et al., 1997; Gersonde, Hodell, Blum, et al., 1999).

The mcd scale and the splice are based on the stratigraphic correlation of whole-core MST and split-core color spectral reflectance (CSR) data (lightness, L*) usually collected at 2- to 8-cm intervals. From the MST, we used magnetic susceptibility (MS), gamma-ray attenuation (GRA) bulk density, and natural gamma radiation (NGR) data (see **"Physical Properties,"** p. 18). Lithostratigraphic events (e.g., volcanic ash layers) and biostratigraphic and magnetostratigraphic datums proved useful as tie points in intervals where correlations were ambiguous.

The raw stratigraphic data were imported into the shipboard Splicer software program (version 2.0) and culled as necessary to avoid incorporating anomalous data influenced by edge effects at section boundaries. Splicer was used to assess the stratigraphic continuity of the recovered sedimentary sequences at each drill site and to construct the mcd scale and splice. Splicer enables the construction of a composite depth scale for each hole at a given site by depth shifting only individual cores to maximize the correlation of MST and CSR data. Because sediments can be distorted by the coring process (the tops of APC cores are generally stretched and the bottoms compressed, although this is lithology dependent) and because depth intervals within cores are not squeezed or stretched, all correlative features cannot be aligned. Correlations among cores from adjacent holes are evaluated visually and statistically. Depth-shifted data are denoted by mcd. A table is presented in each site chapter that summarizes the depth offsets for each core that are necessary to convert mbsf to mcd scales. The mcd for any point within a core equals the mbsf plus the cumulative offset. Correlation at finer resolution is not possible with Splicer since depth adjustments are applied linearly to individual cores; no adjustments, such as squeezing and stretching, are made within cores. Such finer scale adjustment is possible postcruise (e.g., Hagelberg et al., 1995). To assist the reader, all composite section tables and figures from each chapter are presented as either ASCII files, Microsoft Excel files, and/or Synergy Software KaleidaGraph plot files (see the **"ASCII Tables"** and **"Supplementary Materials"** contents lists). This provides the user with greater ability to view, manipulate, graph, and analyze data than is possible within Adobe PDF files, the standard presentation medium.

Ideally, the base of the continuous mcd scale is the bottom of the deepest core recovered from the deepest hole. In practice, however, the base often occurs where core recovery gaps align across all holes. Cores below this interval cannot be directly tied into the overlying and "continuous" mcd. However, below the base of the continuous mcd, cores from two or more holes can often be correlated with each other. At several sites, we constructed discontinuous or "floating" mcd scales for these deeper cores. They are appended to the base of the continuous mcd.

We also used Splicer software to patch together intervals from different holes (based on the mcd scale) to create the splice. The splice does not contain coring gaps, and an effort has been made to minimize inclusion of disturbed sections. The splice is ideally suited to guide core sampling for detailed paleoceanographic studies. A table is presented in each site chapter that summarizes the intervals from each hole used to construct the splice. Like the floating mcd, floating splices were also constructed in cases where sufficiently long sections could be generated but not tied directly to overlying continuous splices.

The length of the mcd scale at a given site is typically ~10% greater than the length of the cored section in any one hole as indicated by the mbsf scale. Although the exact reasons for this are unknown, it is commonly attributed to sediment expansion resulting from decreased overburden pressure in the deeper sections, stretching during the coring process, and other factors (MacKillop et al., 1995). For all sites, the shipboard mcd scale and splices should be considered preliminary and can be improved on with further shore-based work. This is especially true for the floating mcd scales and splice sections.

A certain degree of subjectivity comes into play when constructing a composite depth scale and a splice. If the mcd is built without simulta-

neously considering splice construction, the stratigrapher may focus on maximizing the stratigraphic fit between the entire cores instead of on the portions that eventually become splice segments. In this case, the splice tends to include a large number of small segments from all holes. Our approach was to construct an mcd scale with the goal of creating a splice from the longest possible segments of core and with the smallest number of interhole transitions. This approach has two practical advantages. First, postcruise sampling and sample processing are significantly less complex and therefore less prone to error. Second, this approach allows us to avoid the hole most heavily sampled at sea. This ensures greater availability of material for high-resolution time-series work.

Site 1144 contained intracore voids resulting from gas expansion. Shipboard technicians tried to eliminate or consolidate the voids on the catwalk by drilling gas-escape holes into the core liner and pushing the sediment toward one end of the core, ideally the top (because of the practice of splitting the cores from bottom to top). The voids not removed by this procedure were entered into the JANUS database. These remaining voids introduce a unique problem into the process of developing the mcd scale and splice because the core-splitting process, which involves pulling a cutting wire lengthwise along the section, can dislodge sediments and reposition voids, thus offsetting the split-core CSR measurements from those collected on the whole-core MST (Fig. F1).

F1. The changing position of sediment between voids, p. 31.

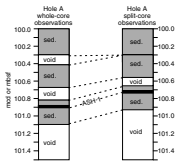

LITHOSTRATIGRAPHY

Visual Core Descriptions

The sediment core graphic descriptions, or barrel sheets, summarize data obtained during shipboard visual inspection of each core. The standard ODP conventions were used for the compilation of the core description forms; the exceptions to these procedures adopted by the Leg 184 Shipboard Scientific Party are described below.

Graphic Lithology Column

All sediment core descriptions were made with the software package AppleCore, using a lithology custom file containing patterns for the standard ODP sediment classification scheme, a modified version of the lithologic classification of Mazzullo et al. (1988). The classification adopted here is outlined in "Rock Classification and Principal Names," p. 8. Sediment type is represented graphically on the core description forms (Fig. F2A) using the patterns illustrated in Figure F2B.

In the graphic lithology column, a maximum of two different lithologies (for interbedded sediments) or three different components (for mixed sediments) can be represented within the same core interval. Percentages of the main lithologic components are rounded to the nearest 5%. Lightness values collected from the Minolta spectrophotometer (see also "Physical Properties," p. 18) are shown in the column to the left of graphic lithology. All core images and graphic lithology columns are included (see the "Core Descriptions" contents list).

F2. Core description form and legend for Leg 184 sites, p. 32.

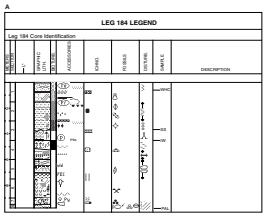

Bioturbation

Five degrees of bioturbation were differentiated (Fig. F2B), following Droser and Bottjer (1986). "Barren" indicates that sediments are undisturbed, whereas primary bedding and structures are fully obliterated by burrowing for "abundant" bioturbation.

Sedimentary Structures

Sedimentary structures include features related to deposition, erosion, and deformation. The location and type of sedimentary structures are shown in the graphic lithology column of the core description form. The symbols used to designate structures found in Leg 184 cores are shown in Figure F2B.

Ichnofossils and Fossils

Ichnofossil and fossil columns indicate the occurrence of ichnofossil genera and major groups of macro- and microfossils. Symbols shown in this column are described in Figure F2B.

Accessories

The accessories column indicates the position of a variety of features such as pyrite, "iron sulfides," lamina, and shell fragments. Symbols shown in this column are described in Figure F2B.

Core Disturbance

Observations of drilling-related disturbance were recorded in the core disturbance column using the symbols shown in Figure F2B. The degree of drilling disturbance in soft and firm sediments is as follows:

1. Slight: bedding contacts are slightly deformed.
2. Moderate: bedding contacts have undergone extreme bowing.
3. Extreme: bedding is completely destroyed; original structure cannot be recognized.

This degree of drilling disturbance is illustrated by the thickness of the symbol (thickest = extreme). In addition to the degree of disturbance, the character of the disturbance is also described as follows (Fig. F2B):

1. Disturbed: bedding is generally intact, but sediment near the core liner is missing or homogenized.
2. Deformed: bedding contacts have been bent.
3. Soupy: sediment is water saturated, and original structure is lost.
4. Flow-in: sediment displays vertical structure caused by coring.
5. Slurry: sediment homogenized during drilling.
6. Biscuit: pieces of partially indurated sediment in the core barrel. The pieces may represent contiguous stratigraphy with millimeter cracks (slight) to small (<3 cm) pieces floating in slurry.
7. Gas expansion: sediment voids or bubbles in sediment caused by gas expansion.

Samples

The positions of samples taken from each core for analysis are indicated by letters in the sample column of the core description form as follows: SS (smear slide), WHC (whole-core sample), PAL (micropaleontology), and IW (interstitial water).

Color

Color was measured with a Minolta CM-2002 spectrophotometer. These measurements were determined on the damp core surface, and GladWrap brand clear plastic film was used to cover the core. The Minolta CM-2002 measures reflected visible light in thirty-one 10-nm-wide bands ranging from 400 to 710 nm. Routine measurements were made at 2-cm spacing for Holes 1143A and 1143B and at 4-cm spacing for all other holes, excluding voids within the sediment section.

Before obtaining measurements from each core, the spectrophotometer was calibrated for white color reflectance; it was "zero calibrated" twice a day, at the beginning of each work shift. The white color calibration was made to avoid variation in color readings stemming from the laboratory environment (temperature, humidity, and background light) and instrument variations.

Lithologic Description

The text description for each core consists of a list of major lithologies followed by a more detailed description of the composition (as determined from smear slides), sedimentary structures, and other notable features. Descriptions and locations of thin, interbedded, or minor lithologies are also included in the text.

Smear Slides

Tables summarizing data from smear-slide analyses are presented (see the "Core Descriptions" contents list). These tables include information about the sample location, whether the sample represents a dominant (D) or a minor (M) lithology in the core, and the estimates of sand, silt, and clay (particle size), together with all identified components (both terrigenous and biogenic material is described and estimated).

Sediment and Rock Classification

Grain Types and Classifications

Grain types in granular sediments and rocks were classified according to composition: biogenic (calcareous and siliceous) and siliciclastic particles. Their definitions are as follows:

1. Biogenic grains are skeletal debris produced in open-marine environments by calcareous microfauna and microflora (foraminifers, pteropods, nannofossils, and associated organisms), and siliceous microfauna and microflora (radiolarians, diatoms, and associated organisms).
2. Siliciclastic grains comprise minerals and rock fragments eroded from plutonic, sedimentary, and metamorphic rocks, as well as

glass shards, rock fragments, and mineral crystals produced by volcanic processes.

Rock Classification and Principal Names

Sediments and rocks were named on the basis of composition and texture using a principal name together with major and minor modifiers. Principal names define the degree of consolidation (induration) and granular sediment class. Table T1 summarizes the granular sediment classification scheme for pelagic and siliciclastic rocks. Composition and texture of cored sediments and rocks were determined aboard ship by visual observation of the core and by visual estimates in smear slides and coarse fractions. Carbonate content was estimated qualitatively in smear slides and quantitatively by coulometric analysis (see "Organic Geochemistry," p. 14).

T1. Lithologic description of sediments and rocks, p. 41.

Induration

Induration of recovered materials was defined as in Gealy et al. (1971). Three classes of induration were used to describe calcareous sediments and rocks:

1. Unlithified: soft sediments that have little strength and are readily deformed under the pressure of a fingernail or the broad blade of a spatula. This corresponds to the term *ooze* for pelagic biogenic sediments.
2. Partially lithified: firm but friable sediments that can be scratched with a fingernail or the edge of a spatula blade. The term *chalk* is used for firm or friable pelagic calcareous material.
3. Lithified: hard, nonfriable cemented rock, difficult or impossible to scratch with a fingernail or the edge of a spatula. The term *limestone* (lithified ooze) is used for pelagic calcareous material.

Two classes of firmness were used to describe siliciclastic sediments and rocks:

1. Soft: sediment core can be split with a wire cutter. Soft terrigenous sediment, pelagic clay, and transitional calcareous sediments are termed sand, silt, or clay.
2. Hard: the core is hard (i.e., consolidated or well indurated) if it must be cut with a hand or diamond saw. For these materials, the suffix *-stone* is added to the soft-sediment name (e.g., sandstone, siltstone, and claystone).

Sediments and Rocks

Principal names used to describe sediments and rocks during Leg 184 are as follows:

1. Clay: unconsolidated authigenic material (>15%) and siliciclastic sediment (lithified examples are termed claystone);
2. Ooze: unconsolidated calcareous and/or siliceous sediment; and
3. Chalk: firm sediment composed predominantly of calcareous grains.

Siliciclastic Sediments and Rocks

For siliciclastic sediments and rocks, texture, structure, and composition are the main criteria for the selection of a principal name. The Udden-Wentworth grain-size scale (Fig. F3) (Wentworth, 1922) defines the grain-size ranges and the names of the textural groups (gravel, sand, silt, and clay) and subgroups (fine sand, coarse silt, etc.). When two or more textural groups or subgroups are present, the principal names appear in order of increasing abundance. Eight major textural categories can be defined on the basis of the relative proportions of sand, silt, and clay (Fig. F4). Distinguishing between some size categories is difficult (e.g., silty clay and clayey silt) without accurate measurements of weight percentages. The terms *conglomerate* and *breccia* are the principal names of gravels with well-rounded and angular clasts, respectively.

F3. Grain-size classification of terrigenous sediments, p. 34.

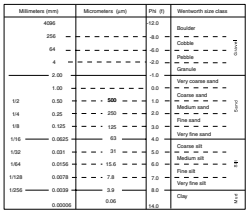

F4. Classification scheme for siliciclastic sediments and rocks, p. 35.

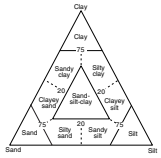

Major and Minor Modifiers

To describe the lithology of the granular sediments and rocks in greater detail, the principal name of a granular sediment class is preceded by major modifiers and followed by minor modifiers (Table T1). Minor modifiers are preceded by the term *with*. The most common uses of major and minor modifiers are to describe the composition and textures of grain types that are present in major (25%–40%) and minor (10%–25%) proportions.

The composition of pelagic grains can be described in greater detail with the major and minor modifiers such as nannofossil, foraminifer, calcareous, and siliceous. The terms *calcareous* and *siliceous* are used to describe sediments that are composed of calcareous or siliceous pelagic grains of uncertain origin.

The textural designations for siliciclastic grains utilize standard major and minor modifiers such as gravel(-ly), sand(-y), silt(-y), and clay(-ey). The character of siliciclastic grains can be described further by mineralogy using modifiers such as quartz, feldspar, glauconite, mica, lithic, or calcareous. In addition, the provenance of rock fragments (particularly in gravels, conglomerates, and breccias) can be described using modifiers such as sed-lithic and meta-lithic. The fabric of a sediment can be described using major modifiers such as grain supported, matrix supported, and imbricated. Generally, fabric terms are useful only when describing gravels, conglomerates, and breccias.

BIOSTRATIGRAPHY

Introduction

During Leg 184, calcareous nannofossils and planktonic foraminifers were studied at six sites, one located on the southern margin and the remainder on the northern continental slope of the South China Sea. With the exception of Site 1148, all sites were triple cored using the APC and XCB systems.

Time Scale

Preliminary ages were assigned to core-catcher samples. Samples from within the cores were examined when a more refined age determination was necessary and when time permitted.

The ages for biostratigraphic datums were compiled mainly from Berggren et al. (1995a, 1995b), Raffi and Flores (1995), Backman and Raffi (1997), Kameo and Bralower (2000), and I. Raffi (unpubl. data). Two Quaternary nannofossil datums, the last occurrence (LO) and first occurrence (FO) of *Gephyrocapsa* (small) acme (Gartner, 1988), were also used. Astrochronologically tuned biostratigraphic datums were used whenever possible (Table **T2**). Estimates of biostratigraphic ages were calibrated against the magnetic polarity time scale of Cande and Kent (1995) and Berggren et al. (1995a, 1995b).

For simplicity, the astrochronologically tuned planktonic foraminifer ages of Berggren et al. (1995a, 1995b) were used for the Holocene to 4.70 Ma. The tuned ages of Chaisson and Pearson (1997), Pearson and Chaisson (1997), and Curry, Shackleton, Richter, et al. (1995) were used for 4.70 to 13.42 Ma. Ages older than 13.42 Ma were untuned and taken from Berggren et al. (1995a, 1995b) (Table **T3**). In addition to the above ages, we also adopted the use of the LO (0.12 Ma; Thompson et al., 1979) and FO (0.40 Ma; Li, 1997) of *Globigerinoides ruber* (pink) as biostratigraphic references.

The biostratigraphic zonation of calcareous nannofossils is based upon the studies of Okada and Bukry (1980) and Martini and Müller (1986). Planktonic foraminifer biostratigraphic zonation is derived from the studies of Blow (1969) (Fig. **F5**).

Ages of Cenozoic chronostratigraphic boundaries were established by Berggren et al. (1995a, 1995b). According to this study, the age of the Pliocene/Pleistocene boundary is 1.77 Ma, the age of the Miocene/Pliocene boundary is 5.32 Ma, and that of the Oligocene/Miocene is 23.80 Ma, as given in Figure **F5.**

Whenever possible, we also tried to note the LO of the benthic foraminifers *Stilostomella*. Several species of this genus disappeared from the global ocean at different latitudes during the interval 1.0–0.6 Ma. For the latitudes of Leg 184, we used 0.75 Ma as the LO of *Stilostomella* (Schönfeld, 1996).

T2. Ages and zonations of calcareous nannofossil datum levels, **p. 42.**

T3. Ages and zonations of planktonic foraminifer datum levels, **p. 43.**

F5. Time scale and biostratigraphic datums, **p. 36.**

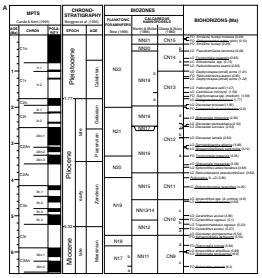

Calcareous Nannofossils

Taxonomic Remarks

Several *Gephyrocapsa* species are commonly used as biostratigraphic markers. However, only two morphological groups, medium and small *Gephyrocapsa* spp., were used during shipboard study. *Gephyrocapsa* (medium) spp. includes specimens from *G. oceanica, G. lumina,* and *G. caribbeanica* with maximum lengths >3.5 µm. *Gephyrocapsa* (small) spp. is used for various *Gephyrocapsa* species with a maximum length <3 µm.

Several *Reticulofenestra* species have been used as Neogene and Quaternary biostratigraphic markers. They are mainly distinguished by coccolith size and the relative magnitude of the central opening. However, some species show a great range of variation in these parameters, causing problems in identification (Backman, 1980; Gallagher, 1987; Young, 1990; Su, 1996). Therefore, only two *Reticulofenestra* species were used as stratigraphic markers during Leg 184. *Reticulofenestra umbilicus* can be easily distinguished from other species by its enormous size. Similarly, *R. pseudoumbilicus* is identified by specimens having a maximum coccolith length >7 µm in its uppermost range (the lower Pliocene), which is in accord with the size of the holotype (Gartner, 1967). Identification of other calcareous nannofossils mainly follows the compilation of Perch-Nielsen (1985).

Methods

Calcareous nannofossils were examined using standard light microscope techniques under crossed polarizers and transmitted light at 1000×–2000× magnification. The degrees of preservation and abundance of calcareous nannofossil species were noted as follows:

VG = very good preservation (no evidence of dissolution and/or overgrowth);
G = good preservation (slight dissolution and/or overgrowth; specimens are identifiable to the species level);
M = moderate preservation (exhibit some etching and/or overgrowth; most specimens are identifiable to the species level); and
P = poor preservation (severely etched or with overgrowth; most specimens cannot be identified at the species and/or generic level).

The relative abundance of individual calcareous nannofossil species is estimated (at 1000× magnification) based on a five-category scheme:

D = dominant (>50%, or 100 specimens per field of view);
A = abundant (10%–50%, or 10–100 specimens per field of view);
C = common (1%–10%, or 1–10 specimens per field of view);
F = few/frequent (0.1%–1%, or 1 specimen per 1–10 fields of view); and
R = rare (<0.1%, or <1 specimen per 10 fields of view).

Planktonic Foraminifers

Taxonomic Remarks

Taxonomic concepts for Neogene and Paleogene taxa follow those of Kennett and Srinivasan (1983), Bolli and Saunders (1985), and South China Sea Branch of Petroleum Corporation of the People's Republic of China et al. (1981).

Methods

Core-catcher samples (plus one sample per section where necessary) were soaked in a weak Calgon/hydrogen peroxide solution, warmed on a hot plate, and washed over a 150-µm mesh sieve (with the exception of Site 1148, where a 63-µm sieve was used for deeper cores). Before washing, each sieve was dipped in a solution of methyl blue dye to identify contaminants from previous samples. Lithified material was crushed to pea size, heated in a Calgon/hydrogen peroxide solution, and then sieved as before. All samples were dried on a hot plate. The dried samples were examined under a binocular microscope, and planktonic foraminifer faunal composition was recorded in qualitative terms based on an assessment of forms observed in a random sample of 200–400 specimens from the >150-µm size fraction. Relative abundances were reported using the following categories:

D = dominant (>30%);
A = abundant (10%–30%);
F = few (5%–10%);

R = rare (1%–5%); and
P = present (<1%).

Preservation of planktonic foraminifer assemblages was recorded as

VG = very good (no evidence of breakage or dissolution);
G = good (>90% of specimens unbroken with only minor evidence of diagenetic alteration);
M = moderate (30%–90% of the specimens unbroken); and
P = poor (strongly recrystallized or dominated by fragments and broken or corroded specimens).

PALEOMAGNETISM

Paleomagnetic studies conducted on the *JOIDES Resolution* during Leg 184 consisted of remanent magnetization measurements of archive-half sections before and after alternating field (AF) demagnetization and measurement of discrete samples obtained from working-half sections.

Instruments and Measurement Procedure

Measurements of remanent magnetization were carried out using an automated pass-through cryogenic direct-current superconducting quantum interference device magnetometer (2-G Enterprises Model 760-R) with an in-line AF demagnetizer (2-G Enterprises Model 2G600), capable of producing peak fields of 80 mT with a 200-Hz frequency. The background noise level of the magnetometer onboard environment is ~3×10^{-10} Am^2. The large volume of core material within the sensing region of the magnetometer, on the order of 100 cm^3, permits the accurate measurements of cores with remanent intensities as weak as ~10^{-5} A/m.

The standard ODP magnetic coordinate system was used (+X = vertical upward from the split surface of archive halves, +Y = left along split surface when looking upcore, +Z = downcore).

The natural remanent magnetization before and after AF demagnetization was routinely measured for all archive-half sections at 4- to 8-cm intervals. Corrections for the end-effect were not applied. Cores from the first hole of each site were generally AF demagnetized at 10 and 20 mT. Other cores were demagnetized by AF at 10, 15, and/or 20 mT, depending on core flow. Discrete samples were demagnetized by AF at five steps: 10, 20, 30, 40, and 50 mT. Seven discrete cube samples were placed on the sample boat at a time, spaced at 20-cm intervals. As many discrete samples as possible were measured given the time limits imposed by core flow. The samples were then divided into two groups and brought back to the Institute for Rock Magnetism and to the Laboratoire des Sciences du Climat et de l'Envirronement for complete paleomagnetic analysis and additional rock and environmental magnetic analysis.

Core Orientation

Orientation of the APC cores was achieved with a Tensor tool mounted on the core barrel. The Tensor tool consists of a three-component fluxgate magnetometer and a three-component accelerometer rig-

idly attached to the core barrel. The information from both sets of sensors allows the azimuth and dip of the hole to be measured as well as the azimuth of the double-line orientation mark on the core liner. Orientation is not usually attempted for the top three cores (~30 mbsf) until the bottom-hole assembly (BHA) is sufficiently stabilized in the sediment. Core orientation by the Tensor tool was relative to magnetic north.

Sampling of Discrete Samples

Oriented discrete samples were taken from the working half of each section (one or two per section) using 8-cm^3 (2 cm × 2 cm × 2 cm = 8 cm^3) plastic cubes and a stainless-steel sampler. The cube fits standard sample holders of paleomagnetic and rock-magnetic instruments. The cubes were capped to prevent dehydration. Orientation arrows for the samples were marked on the bottom of the cube.

Magnetostratigraphy

Where AF demagnetization successfully isolated the primary component of remanent magnetization, paleomagnetic inclinations and declinations relative to magnetic north derived from the Tensor tool were used to assign a magnetic polarity to the stratigraphic column. Interpretations of the magnetic polarity stratigraphy, with constraints from the biostratigraphic data, are presented in the site chapters. The time scale of Berggren et al. (1995) was used.

We encountered several types of secondary magnetization acquired during coring, which sometimes hampered magnetostratigraphic interpretation. Details of the magnetic overprints are presented in the site chapters.

SEDIMENTATION AND ACCUMULATION RATES

We developed preliminary age-depth models for all sites to calculate mass accumulation rates and to aid investigators with sediment sampling strategies. The age-depth control points were extracted from the composite sections for each site; thus, all sedimentation rates are reported in mcd/m.y.

Age-depth models were developed using both biostratigraphic and paleomagnetic control points as presented in **"Biostratigraphy,"** p. 9, and **"Paleomagnetism,"** p. 12. Typically, preference was given first to paleomagnetic data because of their higher sampling resolution, then to nannofossils (over foraminifers) because of generally better stratigraphic resolution. A Stineman function was fit to all data points for a local smoothing effect (geometric weight on current point and 10% of data range). This smoothed curve usually presented a reasonable average when different age datums from the same core-catcher sample were obtained. If the smoothed curve showed abrupt changes in slope as a result of the sampling error (sampling was usually every 10 m), apparent outliers were excluded from the model after discussion with the Leg 184 stratigraphers.

The smoothed age-depth curve was sampled every 5 m to provide the final model for each site. For each depth point x (m), linear sedimentation rates (LSR) were computed for the 10-m window defined by the adjacent depth points:

$$LSR = [depth(x - 5) - depth(x + 5)]/[age(x - 5) - age(x + 5)]\ [m/m.y.].$$

For the calculation of mass accumulation rates (*MAR*), dry density data (*DD* = dry mass/wet volume [in grams per cubic centimeter]) and percent carbonate data (*%CARB*) were linearly interpolated every 5 m. Total mass accumulation was then computed as

$$MAR(\text{total}) = DD \times LSR/10\ [g/cm^2/k.y.],$$

and carbonate accumulation rate as

$$MAR(\text{carbonate}) = \%CARB/100 \times MAR(\text{total})\ [g/cm^2/k.y.].$$

The long-term trends in LSR and MAR are not likely to change significantly based on future work. However, LSR and MAR may change considerably (orders of magnitude) over short intervals (e.g., orbitally controlled glacial or monsoonal cycles) that are not resolved with shipboard sampling and analysis. Also, despite the use of a smoothed age-depth model, the preliminary nature and coarse sampling rate may cause apparent changes in rates that should not be overinterpreted.

ORGANIC GEOCHEMISTRY

The shipboard organic geochemistry program for Leg 184 included (1) real-time monitoring of volatile hydrocarbons (HC) as required by ODP safety regulations; (2) measurement of inorganic carbon (IC) and carbonate content of the sediments; (3) elemental analyses of total carbon, nitrogen, and sulfur; (4) characterization of organic matter (OM) by Rock-Eval and Geofina pyrolysis; and (5) measurement of total chlorin concentration by high-performance liquid chromatography (HPLC) employing fluorescence detection. All methods and instruments used during Leg 184 are described in detail by Emeis and Kvenvolden (1986), Kvenvolden and McDonald (1986), Harris and Maxwell (1995), and Shipboard Scientific Party, 1995.

Volatile Hydrocarbons

For safety and pollution prevention, concentrations and ratios of light HC gases, mainly methane (C_1), ethane (C_2), and propane (C_3), were monitored for each core following the standard headspace sampling method described by Kvenvolden and McDonald (1986; also see **"Headspace Sampling,"** p. 15). Immediately after core retrieval on deck, a sediment sample of ~5 cm^3 was collected using a borer tool, placed in a 21.5-cm^3 glass serum vial, and sealed on deck or immediately in the lab with a septum and metal crimp cap. When consolidated or lithified samples were encountered, chips of material were placed in the vial and sealed. Before gas analyses, the vial was heated at 70°C for a minimum of 20 min. A 5-cm^3 subsample of the headspace gas was extracted from each vial using a 5-cm^3 glass gas syringe for gas chromatography (GC) analysis. When gas pockets and expansion voids were discovered in the core liner, gas samples were collected by penetrating the liner using a 50-cm^3 plastic syringe with a plastic three-way valve connected to a steel penetration tool. Gas HC constituents were analyzed using an HP5890 II gas chromatograph equipped with a 1-cm^3

sample loop, 8 × 1/8 stainless-steel column packed with HayeSep 5, and a flame ionization detector (FID). The C_1/C_2 ratio obtained is particularly important for indicating potential petroleum occurrences; organic-rich sediments commonly have a ratio of >1000, whereas values <200 may indicate potential petroleum generation related to depth and temperature (cf. Stein et al., 1995).

When heavier HC (C_{3+}) were detected, the sample was also analyzed by a natural gas analyzer (NGA) as were selected samples from the southern basin site (Site 1143). The NGA is used to quantify C_1 to C_6 and also nitrogen, oxygen, carbon dioxide, and H_2S (>40 ppmv). Helium was used as a carrier gas. Data acquisition and processing were performed by an HP Chemstation. Chromatographic response was calibrated using commercial standards (Scotty II Analyzed Gases, Scott Specialty Gas Co.) and the results reported in parts per million, by volume (ppmv).

Headspace Sampling

Headspace sampling is an important, but not thoroughly consistent, procedure for shipboard analysis. Sample size and nature can vary, depending on the condition of the core. This can range from soft, organic-rich clay, when the borer tool may be employed, to hard carbonate-rich sediment, from which sample pieces must be cut. Mud generated by the drill bit should be avoided. Coherent cylindrical samples taken by the cork borer generally yielded higher C_1, C_2, and C_3 values per gram of sediment than did discrete pieces of harder sediment. However, this may also reflect the inherent lithologic capacity of the sediment to retain hydrocarbons. It appears not to affect the C_1/C_2 ratio. It is clearly important to employ consistent sample-collection procedures for comparable downcore headspace hydrocarbon analysis.

Additional gas may be released by further heating if necessary for replicate analyses of the same headspace sample. Reheated samples generally yield 10%–50% lower C_{1-3} absolute abundances, but the C_1/C_2 ratios appear unaffected. This may, therefore, be a viable method for verifying anomalous C_1/C_2 values of sediments (e.g., see **"Organic Geochemistry,"** p. 16, in the "Site 1148" chapter).

Inorganic Carbon

Inorganic carbon was determined using a Coulometrics 5011 carbon dioxide coulometer equipped with a System 140 carbonate analyzer. A total of ~10–12 mg of freeze-dried ground sediment was reacted with 2M HCl to liberate CO_2. The change in light transmittance monitored by a photo detection cell controlled the CO_2 titration. The percentage of carbonate was calculated from the inorganic carbon content, assuming that all the CO_2 evolved was derived from dissolution of carbonate by the following equation:

$$\%CaCO_3 = \%IC \text{ (inorganic carbon)} \times 8.33.$$

The amount of carbonate is expressed as weight percent, and no corrections were made for other carbonate minerals.

Elemental Analysis

Total carbon (TC), nitrogen, and sulfur were determined using a Carlo Erba 1500 CNS analyzer, using a new combustion column for each sample batch. An aliquot of 5–15 mg freeze-dried crushed sediment with ~10 mg V_2O_5 oxidant was combusted at 1000°C in a stream of oxygen. Nitrogen oxides were reduced to N_2, and the mixture of N_2, CO_2, H_2O, and SO_2 gases was separated by gas chromatography and detection performed by a thermal conductivity detector (TCD). The H_2 value is not useful because it represents hydrogen from both OM and (clay) minerals. All measurements were calibrated by comparison to pure sulfanilamide as standard. The amount of total organic carbon (TOC) was calculated as the difference between TC and IC (determined from coulometry):

$$\%TOC = \%TC - \%IC.$$

In addition to the carbon analytical data, the C/N ratio can be used to identify the source of the organic matter (fresh marine C/N 6 to 8, degraded marine 8 to 20, and terrestrial C/N >25). However, extensive diagenesis and burial can also increase the value of marine OM to 15 or greater (Meyers, 1994).

Organic Matter Characterization and Maturity Determination

The type of organic matter was characterized by programmed pyrolysis using a Delsi Rock-Eval II system. This method is based on a whole-rock pyrolysis technique designed to identify the type and degree of maturity of OM and to evaluate the petroleum potential of sediments (Espitalié et al., 1986) as well as TOC. The Rock-Eval system includes a temperature program that first releases volatile hydrocarbons (S_1) at 300°C for 3 min. Hydrocarbons are then released via thermal cracking of kerogen (S_2) as the temperature is increased to 550°C at 25°C/min. The S_1 and S_2 hydrocarbons are measured by FID and reported in milligrams per gram dry sediment. The temperature at which the kerogen yields the maximum amount of HC (top of the S_2 peak) provides the parameter T_{max}, used to assess the maturity of the OM. Between 300° and 390°C of the programmed pyrolysis, CO_2 released from the thermal degradation of organic matter (S_3) is trapped and subsequently measured by a TCD and reported in milligrams per gram dry sediment. Rock-Eval parameters facilitate characterization of OM by allowing the following indices to be calculated: hydrogen index (HI = S_2/TOC × 100), oxygen index (OI = S_3/TOC × 100), and S_2/S_3 ratio. In general, high OI values (>100) are an indicator of terrestrial OM or of immature OM of all sources. The production index is defined as $S_1/(S_1 + S_2)$. This value is usually <0.2 in immature rocks; values of 0.3 to 0.4 are typical for samples in the petroleum window (T_{max} 420°–450°C). Values of >0.5 may indicate proximity of migrated HC or trapped petroleum. Interpretation of Rock-Eval OI data is considered to be compromised for samples containing >10% carbonate. Rock-Eval OI values are also unreliable for young and immature OM (<1 Ma or T_{max} <400°C). Samples with <0.5% TOC may not give reliable results because the S_1, S_2, S_3, and S_4 signals are very small.

Chlorin Analysis

Approximately 200 mg (dry weight) of homogenized freeze-dried sediment from each interval was extracted by triple solvent ice-cold sonication (15 min) and centrifugation (3000 rpm; 6 min). The extracts were evaporated to dryness under oxygen-free nitrogen. Volumetric solutions in methanol were prepared and analyzed using an HPLC system consisting of a Waters 501 solvent pump fitted with a Rheodyne 7725 injection valve (20-µL injection loop; flow rate 1 mL/ min) with a Waters 470 tunable scanning fluorescence detector (λ_{ex} = 407 nm; λ_{em} = 662 nm), eluting with methanol (Harris and Maxwell, 1995). The system was operated in the off-column mode, each sample injected twice, and the injection loop flushed with methanol between analyses. Data collection and processing was by an HP Chemstation data program.

INORGANIC GEOCHEMISTRY

Interstitial Waters

Interstitial waters were extracted from whole-round sections 5–10 cm long cut immediately after core retrieval on deck. Samples were gathered with a frequency of one per core in the upper 50 mbsf, and then every third core to the bottom of the hole. After extruding the sediment from the core liner, the surface of each whole-round section was carefully scraped with a spatula to remove potential contamination. Interstitial waters were extracted by placing the sediment in a titanium squeezer and applying pressures up to 40,000 lb (~4150 psi) using a hydraulic press. Water samples were collected into plastic syringes and filtered through 0.45-µm Gelman polysulfone disposable filters. Samples for shipboard analyses were stored in plastic vials. Aliquots for shore-based analyses were stored in heat-sealed acid-washed plastic tubes and/ or glass vials.

Interstitial water analyses followed the procedures outlined by Gieskes et al. (1991). Salinity was measured with a Goldberg optical handheld refractometer. The pH and alkalinity were measured by Gran titration with a Brinkmann pH electrode and a Metrohm autotitrator. The Cl^- concentration was measured by titration. The H_4SiO_4, HPO_4^{2-}, and NH_4^+ concentrations were measured by spectrophotometric methods with a Milton Roy Spectronic 301 spectrophotometer. The K^+, Mg^{2+}, Ca^{2+}, and SO_4^{2-} concentrations were calculated by ion chromatography using a Dionex DX-100 instrument. The Li^+ and Sr^{2+} concentrations were measured by flame atomic absorption spectrophotometry using a Varian SpectrAA-20. The Mg^{2+} and Ca^{2+} concentrations were gauged by titration at Site 1143 to assess the reproducibility of the results from ion chromatography.

We used sample replicates (NH_4^+ and HPO_4^{2-}) and the International Association of Physical Sciences Organizations standard seawater (all other elements) to determine 1 σ standard deviation. The standard deviations were alkalinity, <1.5%; Cl^-, 1 mM; Ca^{2+}, 0.9 mM; Mg^{2+}, 0.8 mM; Si^+, 0.7 µM; NH_4^+, 0.2 mM; K^+, 0.8 mM; SO_4^{2-}, 0.4 mM; Na^+, 5 mM; HPO_3^{2-}, 0.1 µM; Li^+, 1 µM; and Sn^{2+}, 2 µM. Reproducibility for Mg^{2+} and Ca^{2+} concentrations measured by titration was 0.03 mM.

PHYSICAL PROPERTIES

Introduction

Bulk density (GRA), compressional wave velocity (*P*-wave velocity), MS, and NGR were measured on whole-core sections using the MST. These closely spaced (generally 2–5 cm) measurements are used to characterize lithologic changes and to correlate cores from multiple holes to construct a continuous stratigraphic section (see "Composite Section," p. 3). Thermal conductivity measurements using the needle-probe method were taken on whole-core sections at discrete intervals, particularly within intervals where downhole temperature measurements were performed. Heat flow was determined from four to five borehole temperature measurements as well as thermal conductivity measurements on whole cores. After the core was split, further physical properties measurements were made on the working half. These included compressional wave velocity, moisture and density (MAD), and color reflectance measurements using the Minolta CM-2002 spectrophotometer. Samples for MAD measurements normally were extracted at regularly spaced intervals. However, additional samples were taken in thin lithologic units that would have been missed by regular sampling patterns. A detailed description of most of the techniques used is given in the ODP physical properties handbook (Blum, 1997) and are only summarized here.

Multisensor Track

Whole-core sections were run through the MST after they had equilibrated to the ambient laboratory room temperature (21°–25°C, as measured at the top of the section). The MST data were sampled at the highest sampling rate possible given the time constraints of coring operations. Generally, a 5-cm sampling interval and 4-s sampling periods were the optimal settings.

The quality of core-logging data and the accuracy of the nominal values are degraded if the core liner is not completely filled and/or the core is disturbed. However, general downhole trends may still be used for core-to-core and core-to-well log correlation.

Magnetic Susceptibility

Magnetic susceptibility was measured using a Bartington meter (model MS2C), which has an 80-mm internal-diameter loop and a low-sensitivity setting of 1.0 Hz. The mean value of the 4-s measurements was stored in the database. Wet volume-normalized SI units were calculated from the sensor readings by multiplication with a factor of 0.68×10^{-5}, where the factor is related to the coil-to-diameter ratio (Blum, 1997). This factor is approximate; the true SI value may differ by a constant offset of up to half an order of magnitude, depending upon sediment diameter (e.g., APC and XCB diameters differ), core liner thickness, and liner deformation. Magnetic susceptibility was the most useful record for core-to-core correlation and composite depth construction.

GRA Bulk Density

Estimates of bulk-sediment density were obtained from GRA measurements. These estimates are based on the comparison of the attenuation of gamma rays through the cores with attenuation through calibration standards. These standards consist of an aluminum rod with different diameters within a water-filled core liner (Blum, 1997). This calibration incorporates the lower Compton scattering in water and a correction for the core liner.

Velocity

The *P*-wave logger (PWL) on the MST transmits a 500-kHz compressional wave pulse through the core. The transmitting and receiving transducers are aligned perpendicular to the long axis of the core (y-direction). A pair of displacement transducers monitors the distance between the compressional wave transducers. The PWL is the MST device most sensitive to core condition and was the first to be turned off if core condition deteriorated. Data quality was assessed by examining arrival times and amplitudes of the received pulses. Calibration of the displacement transducer and measurement of electronic delay within the PWL circuitry were performed using a series of acrylic blocks of known thickness and *P*-wave traveltime. The validity of the calibration was checked by measuring the *P*-wave velocity through a section of liner filled with distilled water. However, because of instrument problems, the PWL records are very noisy and need to be specially processed. This will be done postcruise. The data from the PWL are not further discussed in this report but are available from the ODP JANUS database (see the **"Related Leg Data"** contents list).

Natural Gamma Radiation

The NGR system records the radioactive decay of ^{40}K, ^{232}Th, and ^{238}U. Although 256-channel spectra were recorded, only the total counts were used for shipboard analysis. The four detectors of the NGR device were tuned using a ^{232}Th source at the beginning of the leg. Thorium and K were used about once per week to assign the appropriate channels to their characteristic emission energies. Background radiation was determined by measuring a water-filled core liner.

Thermal Conductivity

Thermal conductivity is the measure of a material's ability to transmit heat by molecular conduction and is required for geothermal heat-flow determinations. Thermal conductivity of soft sediments was measured using the needle-probe method, in full-space configuration (Von Herzen and Maxwell, 1959; Blum, 1997). At least one measurement per core was made, usually near the middle of the core, after the cores had equilibrated to laboratory temperature (~3–4 hr after recovery). Additional thermal conductivity measurements were made in intervals where downhole temperature measurements had been run. Data are reported in units of W/(m·K).

The TK04 (Teka, Berlin) was used for the thermal conductivity measurements. A needle probe (#V00594), containing a heater wire and a calibrated thermistor, was inserted into the sediment through a small hole drilled in the core liner. Three measuring cycles were automatically

performed at each location. At the beginning of each cycle, a self-test, which included a drift study, was conducted. Once the samples were equilibrated, the heater circuit was closed, and the temperature rise in the probes was recorded. Thermal conductivities were calculated from the rate of temperature rise while the heater current was flowing. Temperatures measured during the first 150 s of the heating cycle were fitted to an approximate solution of a constantly heated line source (Kristiansen, 1982; see Blum, 1997, for details). Errors are between 5% and 10%. Corrections were not attempted for in situ temperature or pressure effects.

Moisture and Density

Bulk density, grain density, water content, porosity, dry density, and void ratio were calculated from measurements of wet and dry masses and dry volumes. Samples of ~10 cm^3 were taken from split cores at sampling intervals of 1.5 m. However, where frequent lithologic changes occurred, denser sampling was done to ensure measurements from all lithologies throughout the core.

Sample mass was determined using a Scientech electronic balance. The sample mass was counterbalanced by a known mass, so that only mass differences of usually <2 g were measured. The balance was also equipped with a computer-averaging system that corrected for ship accelerations. Dry mass was measured from samples oven-dried at 110°C ±5°C for 24 hr and cooled in a desiccator for 2 hr.

Dry volumes were determined using a helium-displacement Quantachrome Penta-Pycnometer. Sample volume measurements were repeated up to three times until the last three measurements had <0.01% standard deviation. A purge time of 3–5 min was used before each run. A reference sphere of known volume was run with each group of four samples during all the measurements. The standard was rotated systematically among cells to check for errors.

Compressional Wave (*P*-wave) Velocity on Split Cores

In addition to the velocity measurements taken with the PWL on the MST, compressional wave velocity was measured on split-core sections.

For soft sediments, the *P*-wave velocity was determined with the PWS (*P*-wave velocity sensor)1 in z-direction and PWS2 in y-direction. Two transducer pairs were inserted manually into the sediment and the traveltime of a sonic signal between the sensors was measured. *P*-wave velocity is calculated using the measured traveltime and the distance between the transducers. Calibration of the system was performed according to Blum (1997).

An external digital thermometer was used to record core temperature. The values are stored in the database but are not used for shipboard reporting.

The PWS3 contact probe system measured the traveltime of a 500-kHz signal in two modes depending on the sediment consistency. In the split-core mode, the section liner rests on the bottom transducer, and the upper transducer is lowered manually onto the core surface. *P*-wave velocity is measured parallel to the sediment bedding (x-direction). In the specimen mode (for hard sediments), the oriented sample is placed directly between the transducers in the desired orientation (x-, y-, or z-direction; ODP definitions of directions are illustrated in Blum,

1997). Sample thickness was measured directly by a digital multimeter. Measurement frequency was the same as that used for MAD samples.

Delay times for the velocity transducers were estimated by linear regression of traveltime vs. distance for a series of aluminum and lucite standards. Velocity data recorded in the JANUS database are uncorrected for in situ temperature and pressure (such corrections can be made using relationships in Wyllie et al., 1956).

Only after completion of Site 1145 was it discovered that, because of an operational error, the distance between the transducers had been measured incorrectly. Therefore, PWS3 velocity values are not correct for Sites 1143 and 1145 and can only be regarded with extreme caution. (At Site 1144, no *P*-wave velocities could be measured because of the core conditions.) The problem was discovered and fixed at Site 1146 and all PWS3 values for Sites 1146, 1147, and 1148 are correct.

Color Reflectance

Quantitative estimates of sediment diffuse spectral reflectance and sediment color were generated by the shipboard sedimentologists using a handheld Minolta CM-2002 spectrophotometer. The new AMST core logger was not usable because of software problems. The archive halves were wrapped in GladWrap plastic film to protect the spectrophotometer opening. The CM-2002 was operated and calibrated according to the Minolta CM-2002 users' manual (Minolta Camera Co., 1991). The Minolta color data are presented in uncorrected form in this volume and are available from the ODP JANUS database (see the **"Related Leg Data"** contents list).

WIRELINE LOGGING

Introduction

Downhole logs are used to determine physical, chemical, and structural properties of formations penetrated by drilling. The data are rapidly collected, are continuous with depth, and measure in situ properties; they can be used to interpret the formation's stratigraphy, lithology, and mineralogy. In intervals of no core recovery, logs provide the only means to describe the formation. Where XCB core recovery is poor, logs will often supply superior physical and chemical measurements of the interval compared to those of the core; where core recovery is good, log data complement core data. Logs also provide a link between core and seismic sections: sonic velocity logs improve depth to traveltime conversions, and synthetic seismograms may be compared directly to the seismic sections.

Logging tools were joined together in "tool strings" (Fig. **F6**), so that several measurements could be made during each logging run. The tool strings were lowered to the bottom of the borehole on a wireline cable, and data were logged as the tool string was pulled back up the hole. Repeat runs were made in some holes to improve coverage and confirm the accuracy of log data. During logging runs, a wireline heave compensator was employed to minimize the effect of ship's heave (caused by sea swell) on the motion and position of the tool string in the borehole. Not all tool strings were run in each hole; individual site chapters give details of logging strings deployed at each site. Examples of the use of

F6. Schematic illustration of the configurations of tool strings, **p. 39.**

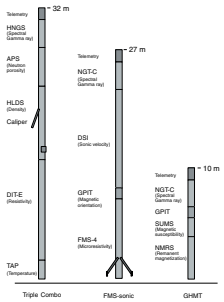

downhole logs for paleoceanographic objectives are given in Lyle, Koizumi, Richter, et al. (1997).

About the Acronyms

Schlumberger tools and tool measurements are identified by three- or four-letter acronyms (Table T4). Often the acronym has no convenient translation, and the acronym itself becomes the name of the tool or measurement. In the site chapters we have tried to avoid the use of acronyms if practical. For example, "density" instead of "RHOM" is used for the bulk density log. The GHMT (geological high-resolution magnetic tool) is always called the GHMT, and the FMS (Formation MicroScanner) is always called the FMS. The advantage of using the acronyms is that the tool, units, and measurement methods are completely specified by the three- or four-letter acronyms.

T4. Logging tool and measurement acronyms and units of measurement, p. 46.

Logging Tools and Tool Strings

During Leg 184, we deployed the following three logging strings (Fig. F6; Table T5):

1. The triple-combination (resistivity, density, and porosity) tool string consists of the dual-induction tool (DIT), the hostile environment lithodensity sonde (HLDS), and the accelerator porosity sonde (APS). The hostile environment natural gamma-ray sonde (HNGS) was included at the top, and the Lamont-Doherty Earth Observatory (LDEO) high-resolution temperature/acceleration/pressure tool (TAP) was attached to the base of this tool string. Because low resistivities were encountered in Leg 184 holes, we used the DIT.
2. The FMS-sonic tool string consists of the FMS, the general-purpose inclinometer tool (GPIT), and the dipole sonic imager (DSI). The natural gamma-ray tool (NGT) was included at the top of this tool string.
3. The GHMT is composed of the nuclear magnetic remanence sonde (NMRS) and the susceptibility measurement sonde (SUMS). The NGT was again positioned at the top of this tool string.

T5. Specifications of the logging tools grouped into tool strings, p. 47.

Log data from the NGT placed at the top of all tool strings provide a common basis for correlation of several logging runs and for depth shifting all logs. A telemetry unit is placed at the very top of each string.

Principles and Uses of the Tools

Brief descriptions of individual logging tools used during Leg 184, including their geological applications and data-quality controls, are given in the following text. The properties of the formation measured by each tool, the sample intervals used, and the precision of the measurements made (including the vertical resolution and depth of investigation into the formation wall at typical logging speeds) are summarized in Table T5. More detailed descriptions of individual logging tools and their geological applications can be found in Ellis (1987), Goldberg (1997), Lovell et al. (1998), Rider (1996), Schlumberger (1989, 1994a, 1994b, 1995), Serra (1984, 1986, 1989), Timur and Toksöz

(1985), and the LDEO–Borehole Research Group (BRG) *Wireline Logging Services Guide* (1994).

The HNGS and NGT measure the natural gamma radiation from isotopes of potassium, thorium, and uranium in the sediment surrounding the tool. High K and Th values indicate greater clay concentrations, and increased U values often indicate the presence of organic matter. The NGT and HNGS also provide a measure of the total or spectral gamma-ray signature (in American Petroleum Institute gamma radiation units [gAPI]) and uranium-free or computed gamma ray (gAPI units).

The APS emits fast neutrons, which are slowed by hydrogen in the formation, and the energy of the rebounded neutrons is measured at detectors spaced along the tool. Most hydrogen is in the pore water, hence porosity may be derived. Hydrogen bound in minerals such as clays also contributes to the measurement, however, so that the raw porosity value is often overestimated. The neutrons slowed to thermal energies are captured by nuclei, especially those of chlorine and the heavier elements; this effect is measured by the APS as the neutron capture cross section, Σ_f.

The HLDS emits high-energy gamma rays, which are scattered in the formation. The bulk density is derived from the energy of the returning gamma rays. Porosity may also be derived from this bulk density, if the matrix density is known. In addition, the HLDS measures the photoelectric effect (PEF; absorption of low-energy gamma rays), which varies according to the chemical composition of the sediment (e.g., PEF of pure calcite = 5.08, illite = 3.03, quartz = 1.81, and kaolinite = 1.49 barn/e^-). The HNGS, APS, and HLDS together comprise the integrated porosity-lithology tool.

The DIT measures the formation electrical resistivity at three different penetration depths: by electromagnetic induction for the deep and medium resistivity, and by current balancing for the shallow resistivity. Porosity, fluid salinity, clay content, grain size, and gas hydrate content all contribute to the resistivity.

The full specifications of the TAP tool are described in Table **T6.** Temperature (recorded by high-precision thermistors) and pressure are measured every second. Tool acceleration is recorded four times per second. Data are recorded as a function of time and correlated with depth based on a synchronized time-wireline cable depth record and on pressure recordings.

T6. LDEO-TAP tool specifications, **p. 48.**

The DSI employs a combination of monopole and dipole transducers (see Fig. **F7**) to make accurate measurements of sonic wave propagation in a wide variety of lithologies (Schlumberger, 1995). It replaces the more commonly used array sonic tool. In addition to robust and high-quality determination of compressional wave velocity, the DSI excites a flexural mode in the borehole that can be used to determine shear-wave velocity in all types of formations. When the formation shear velocity is less than the borehole fluid velocity, particularly in unconsolidated sediments, the flexural wave travels at shear-wave velocity and is the most reliable means to estimate a shear velocity log. The configuration of the DSI also allows recording of cross-line dipole waveforms. These modes can be used to estimate shear-wave splitting caused by preferred mineral and/or structural orientations in consolidated formations. A low-frequency source enables Stoneley waveforms to be acquired as well.

F7. Schematic illustration of the DSI, **p. 40.**

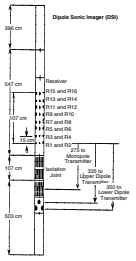

The FMS produces high-resolution images of the microresistivity of the borehole wall. The tool has four orthogonally oriented pads, each with 16 button electrodes that are pressed against the borehole wall

(Serra, 1989). Roughly 30% of a 25-cm diameter borehole is imaged. The vertical resolution is ~5 mm, allowing features such as clasts, thin beds, fractures, and veins to be imaged. The images are oriented, so that both strike and dip can be obtained for the sediment fabric. The FMS images have proved particularly valuable in the interpretation of sedimentary structures during previous ODP legs and have been used to identify cyclical stacking patterns in carbonates (Eberli, Swart, Malone, et al., 1997), soft sediment slumping (Kroon, Norris, Klaus, et al., 1998), turbidite deposits (Lovell et al., 1998), cross-beds (Hiscott et al., 1992), and facies changes (Serra, 1989). Detailed interpretation of FMS images in combination with other log and core data will be carried out post-cruise at LDEO-BRG, at Leicester University Borehole Research (LUBR), and at Laboratoire de Mesures en Forage (LMF), Cerege, Aix-en-Provence (France).

The GPIT was included in the FMS-sonic tool string to calculate tool acceleration and orientation during logging. The GPIT contains a triple-axis accelerometer and a triple-axis magnetometer. This tool records the orientation of the FMS images and allows more precise determination of log depths than can be determined from cable length, which may be stretched and/or affected by ship heave.

The GHMT normally consists of a high-sensitivity total magnetic field sensor (NMRS) coupled with a magnetic susceptibility sensor (SUMS). The NMRS measures the total magnetic field, using a proton precession magnetometer. A polarity stratigraphy can usually be determined by comparing the variations in total field and susceptibility downhole, after removing the background geomagnetic reference field and the effect of the pipe. The SUMS measures magnetic susceptibility by means of low-frequency induction in the surrounding sediment. It responds to magnetic minerals (mainly magnetite and "iron sulfides"), which are often contained in the detrital sediment fraction and can be a proxy for paleoenvironmental change. The GHMT measurements for magnetic susceptibility and earth conductivity are displayed in instrument units (IU).

Logging Operations

Borehole Preparation

Before logging, holes were flushed of debris by circulating heavy viscous drilling fluid (sepiolite mud and seawater) through the hole. The BHA was then pulled up to between 80 and 110 mbsf, then run down the hole again to ream out borehole irregularities and stabilize borehole walls. The hole was then filled with a sepiolite mud pill and the BHA raised to 80–110 mbsf.

Data Recording and Processing

Data from each logging run were recorded, stored digitally, and monitored in real time using the Schlumberger Multitask Acquisition and Imaging System 500. After logging at each hole, data were transferred to the shipboard downhole measurements laboratory for preliminary processing and interpretation. The FMS image data were interpreted using Schlumberger's Geoframe 3.1.4 software package. Sonic and density data were deciphered using GeoQuest's IESX software package to establish the seismic-to-borehole tie. Logs from the shipboard processed data

were plotted as depth-related curves (or images), representing the physical and chemical properties of the strata penetrated.

Soon after each hole was logged, wireline log data were transmitted to LDEO-BRG for processing using a FFASTEST satellite high-speed data link. Data processing at LDEO-BRG includes (1) depth shifting all logs relative to a common datum (i.e., mbsf), (2) corrections specific to individual tools, and (3) quality control and rejection of unrealistic or spurious values. Once processed at LDEO-BRG, log data were transmitted back to the ship. Log curves of LDEO-BRG–processed data were then replotted on board for refining interpretations (see **"Wireline Logging,"** p. 26, in the "Site 1143" chapter; **"Wireline Logging,"** p. 22, in the "Site 1144" chapter; **"Wireline Logging,"** p. 22, in the "Site 1146" chapter; and **"Wireline Logging,"** p. 26, in the "Site 1148" chapter). Further postcruise processing of the log data from the FMS and GHMT will be performed at LMF.

Postcruise processed acoustic, caliper, density, gamma-ray, magnetic, neutron porosity, resistivity, and temperature data in ASCII format are available directly from the LDEO-BRG Internet Web site (see the **"Related Leg Data"** contents list). A summary of logging highlights is also posted on the LDEO-BRG Web site at the end of each leg. Downhole logging aboard the *JOIDES Resolution* is provided by LDEO-BRG in conjunction with LUBR, LMF, the University of Aachen, the University of Tokyo, and Schlumberger well-logging services.

Log Data Quality

A major factor influencing the quality of log data is the condition of the borehole. If the borehole diameter is variable over short intervals (resulting from washouts during drilling, clay swelling, or borehole wall collapse), there may be data acquisition problems for tools that require good contact with the wall (i.e., FMS and density and porosity logging tools). Measurements such as resistivity and sonic velocity that penetrate deep into formation walls and do not require contact with the borehole wall are generally less sensitive to borehole conditions. The quality of boreholes was improved by minimizing the circulation of drilling fluid, flushing the borehole to remove debris, and logging as soon as possible after drilling and conditioning were completed. Controls affecting data quality from each tool are discussed in the descriptions in **"Log Depth Scales,"** p. 25.

Log Depth Scales

The depth of each logged measurement is calculated from the length of the logging cable, minus the cable length to the seafloor (the seafloor is identified by an abrupt reduction in gamma-ray counts at the water/sediment interface). Discrepancies between the drill-pipe depth, the log depth, and the total core length may occur because of core expansion, incomplete core recovery, drill-pipe stretch in the case of drill-pipe depth, incomplete heave compensation, cable stretch (~1 m/km), and cable slip in the case of log depth. Tidal changes in sea level may also have an effect. Thus, small but significant differences may occur between drill-pipe depth and cable depth, which should be taken into account when using the logs. Sagan, a new software module for depth shifting spliced core data to the wireline log depth scale, was used for the second time (its first use was during Leg 182). Sagan was developed by Peter deMenocal and Ann Esmay of LDEO for ODP Logging Services

Space. The beta version of the Sagan software package was used to convert core mcd into mbsf as measured by wireline logging (see "Composite Section," p. 3).

REFERENCES

Backman, J., 1980. Miocene-Pliocene nannofossils and sedimentation rates in the Hatton-Rockall Basin, NE Atlantic Ocean. *Stockholm Contrib. Geol.,* 36:1–91.

Backman, J., and Raffi, I., 1997. Calibration of Miocene nannofossil events to orbitally tuned cyclostratigraphies from Ceara Rise. *In* Shackleton, N.J., Curry, W.B., Richter, C., and Bralower, T.J. (Eds.), *Proc. ODP, Sci. Results,* 154: College Station, TX (Ocean Drilling Program), 83–99.

Berggren, W.A., Hilgen, F.J., Langereis, C.G., Kent, D.V., Obradovich, J.D., Raffi, I., Raymo, M.E., and Shackleton, N.J., 1995. Late Neogene chronology: new perspectives in high-resolution stratigraphy. *Geol. Soc. Am. Bull.,* 107:1272–1287.

Berggren, W.A., Kent, D.V., Swisher, C.C., III, and Aubry, M.-P., 1995a. A revised Cenozoic geochronology and chronostratigraphy. *In* Berggren, W.A., Kent, D.V., Aubry, M.-P., and Hardenbol, J. (Eds.), *Geochronology, Time Scales and Global Stratigraphic Correlation*. Spec. Publ.—Soc. Econ. Paleontol. Mineral. (Soc. Sediment. Geol.), 54:129–212.

Blow, W.H., 1969. Late middle Eocene to Recent planktonic foraminiferal biostratigraphy. *In* Brönnimann, P., and Renz, H.H. (Eds.), *Proc. First Int. Conf. Planktonic Microfossils, Geneva, 1967:* Leiden (E.J. Brill), 1:199–422.

Blum, P., 1997. Physical properties handbook: a guide to the shipboard measurements of physical properties of deep-sea cores. *ODP Tech. Note,* 26.

Bolli, H.M., and Saunders, J.B., 1985. Oligocene to Holocene low latitude planktic foraminifera. *In* Bolli, H.M., Saunders, J.B., and Perch-Nielsen, K. (Eds.), *Plankton Stratigraphy:* Cambridge (Cambridge Univ. Press), 155–262.

Cande, S.C., and Kent, D.V., 1995. Revised calibration of the geomagnetic polarity timescale for the Late Cretaceous and Cenozoic. *J. Geophys. Res.,* 100:6093–6095.

Chaisson, W.P., and Pearson, P.N., 1997. Planktonic foraminifer biostratigraphy at Site 925: middle Miocene–Pleistocene. *In* Shackleton, N.J., Curry, W.B., Richter, C., and Bralower, T.J. (Eds.), *Proc. ODP, Sci. Results,* 154: College Station, TX (Ocean Drilling Program), 3–31.

Curry, W.B., Shackleton, N.J., Richter, C., et al., 1995. *Proc. ODP, Init. Repts.,* 154: College Station, TX (Ocean Drilling Program).

Droser, M.L., and Bottjer, D.J., 1986. A semiquantitative field classification of ichnofabric. *J. Sediment. Petrol.,* 56:558–559.

Eberli, G.P., Swart, P.K., Malone, M.J., et al., 1997. *Proc. ODP, Init. Repts.,* 166: College Station, TX (Ocean Drilling Program).

Ellis, D.V., 1987. *Well Logging for Earth Scientists:* New York (Elsevier).

Emeis, K.-C., and Kvenvolden, K.A., 1986. Shipboard organic geochemistry on *JOIDES Resolution*. *ODP Tech. Note,* 7.

Espitalié, J., Deroo, G., and Marquis, F., 1986. La pyrolyse Rock-Eval et ses applications, Partie III. *Rev. Inst. Fr. Pet.,* 41:73–89.

Farrell, J.W., and Janecek, T.R., 1991. Late Neogene paleoceanography and paleoclimatology of the northeast Indian Ocean (Site 758). *In* Weissel, J., Peirce, J., Taylor, E., Alt, J., et al., *Proc. ODP, Sci. Results,* 121: College Station, TX (Ocean Drilling Program), 297–355.

Gallagher, L., 1987. *Reticulofenestra:* a critical review of taxonomy, structure and evolution. *In* Crux, J.A., and van Heck, S.E. (Eds.), *Nannofossils and Their Applications:* Chichester (Ellis Horwood), 41–75.

Gartner, S., 1967. Calcareous nannofossils from Neogene of Trinidad, Jamaica, and Gulf of Mexico. *Univ. Kansas Paleontol. Contrib.,* 29:1–7.

————, 1988. Paleoceanography of the Mid-Pleistocene. *Mar. Micropaleontol.,* 13:23–46.

Gealy, E.L., Winterer, E.L., and Moberly, R., Jr., 1971. Methods, conventions, and general observations. *In* Winterer, E.L., Riedel, W.R., et al., *Init. Repts. DSDP,* 7 (Pt. 1): Washington (U.S. Govt. Printing Office), 9–26.

Gersonde, R., Hodell, D.A., Blum, P., et al., 1999. *Proc. ODP, Init. Repts.,* 177 [CD-ROM]. Available from: Ocean Drilling Program, Texas A&M University, College Station, TX 77845-9547, U.S.A.

Gieskes, J.M., Gamo, T., and Brumsack, H., 1991. Chemical methods for interstitial water analysis aboard *JOIDES Resolution. ODP Tech. Note,* 15.

Goldberg, D., 1997. The role of downhole measurements in marine geology and geophysics. *Rev. Geophys.,* 35:315–342.

Hagelberg, T., Shackleton, N., Pisias, N., and Shipboard Scientific Party, 1992. Development of composite depth sections for Sites 844 through 854. *In* Mayer, L., Pisias, N., Janecek, T., et al., *Proc. ODP, Init. Repts.,* 138 (Pt. 1): College Station, TX (Ocean Drilling Program), 79–85.

Hagelberg, T.K., Pisias, N.G., Shackleton, N.J., Mix, A.C., and Harris, S., 1995. Refinement of a high-resolution, continuous sedimentary section for studying equatorial Pacific Ocean paleoceanography, Leg 138. *In* Pisias, N.G., Mayer, L.A., Janecek, T.R., Palmer-Julson, A., and van Andel, T.H. (Eds.), *Proc. ODP, Sci Results,* 138: College Station, TX (Ocean Drilling Program), 31–46.

Harris, P.G., and Maxwell, J.R., 1995. A novel method for the rapid determination of chlorin concentrations at high stratigraphic resolution in marine sediments. *Org. Geochem.,* 23:853–856.

Hiscott, R.N., Colella, A., Pezard, P., Lovell, M.A., and Malinverno, A., 1992. Sedimentology of deep-water volcaniclastics, Oligocene Izu-Bonin forearc basin, based on formation microscanner images. *In* Taylor, B., Fujioka, K., et al., *Proc. ODP, Sci. Results,* 126: College Station, TX (Ocean Drilling Program), 75–96.

Jansen, E., Raymo, M.E., Blum, P., et al., 1996. *Proc. ODP, Init. Repts.,* 162: College Station, TX (Ocean Drilling Program).

Kameo, K., and Bralower, T.J., 2000. Neogene calcareous nannofossil biostratigraphy of Sites 998, 999, and 1000, Caribbean Sea. *In* Leckie, R.M., Sigurdsson, H., Acton, G.D., and Draper, G. (Eds.), *Proc. ODP, Sci. Results,* 165: College Station, TX (Ocean Drilling Program), 3–17.

Kennett, J.P., and Srinivasan, M.S., 1983. *Neogene Planktonic Foraminifera: A Phylogenetic Atlas:* Stroudsburg, PA (Hutchinson Ross).

Kristiansen, J.I., 1982. The transient cylindrical probe method for determination of thermal parameters of earth materials [Ph.D. dissert.]. Aaehus Univ.

Kvenvolden, K.A., and McDonald, T.J., 1986. Organic geochemistry on the *JOIDES Resolution*—an assay. *ODP Tech. Note,* 6.

Lamont-Doherty Earth Observatory-Borehole Research Group, 1994. *Wireline Logging Services Guide:* Lamont-Doherty Earth Observatory-Borehole Research Group.

Li, B., 1997. Paleoceanography of the Nansha Area, southern South China Sea since the last 700,000 years [Ph.D. dissert.]. Nanjing Inst. Geol. Paleontol., Academica Sinica, Nanjing, China. (in Chinese, with English abstract)

Lovell, M.A., Harvey, PK., Brewer, T.S., Williams, C., Jackson, P.D., and Williamson, G., 1998. Application of FMS images in the Ocean Drilling Program: an overview. *In* Cramp, A., MacLeod, C.J., Lee, S.V., and Jones, E.J.W. (Eds.), *Geological Evolution of Ocean Basins: Results from the Ocean Drilling Program.* Geol. Soc. Spec. Publ. London, 131:287–303.

Lyle, M., Koizumi, I., Richter, C., et al., 1997. *Proc. ODP, Init. Repts.,* 167: College Station, TX (Ocean Drilling Program).

MacKillop, A.K., Moran, K., Jarrett, K., Farrell, J., and Murray, D., 1995. Consolidation properties of equatorial Pacific Ocean sediments and their relationship to stress history and offsets in the Leg 138 composite depth sections. *In* Pisias, N.G., Mayer, L.A., Janecek, T.R., Palmer-Julson, A., and van Andel, T.H. (Eds.), *Proc. ODP, Sci. Results,* 138: College Station, TX (Ocean Drilling Program), 357–369.

Martini, E., and Müller, C., 1986. Current Tertiary and Quaternary calcareous nannoplankton stratigraphy and correlations. *Newsl. Stratigr.,* 16:99–112.

Mazzullo, J.M., Meyer, A., and Kidd, R.B., 1988. New sediment classification scheme for the Ocean Drilling Program. *In* Mazzullo, J., and Graham, A.G. (Eds.), *Handbook for Shipboard Sedimentologists*. ODP Tech. Note, 8:45–67.

Meyers, P.A., 1994. Preservation of elemental and isotopic source identification of sedimentary organic matter. *Chem. Geol.,* 144:289–302.

Minolta Camera Co, 1991. *Spectrophotometer CM-2002 Instruction Manual:* Osaka, Japan (Minolta Camera Co.).

Norris, R.D., Kroon, D., Klaus, A., et al., 1998. *Proc. ODP, Init. Repts.,* 171B: College Station, TX (Ocean Drilling Program).

Okada, H., and Bukry, D., 1980. Supplementary modification and introduction of code numbers to the low-latitude coccolith biostratigraphic zonation (Bukry, 1973; 1975). *Mar. Micropaleontol.,* 5:321–325.

Pearson, P.N., and Chaisson, W.P., 1997. Late Paleocene to middle Miocene planktonic foraminifer biostratigraphy of the Ceara Rise. *In* Shackleton, N.J., Curry, W.B., Richter, C., and Bralower, T.J. (Eds.), *Proc. ODP, Sci. Results,* 154: College Station, TX (Ocean Drilling Program), 33–68.

Perch-Nielsen, K., 1985. Mesozoic calcareous nannofossils. *In* Bolli, H.M., Saunders, J.B., and Perch-Nielsen, K. (Eds.), *Plankton Stratigraphy:* Cambridge (Cambridge Univ. Press), 329–426.

Prell, W.L., 1982. Oxygen and carbon isotope stratigraphy for the Quaternary of Hole 502B: evidence for two modes of isotopic variability. *In* Prell, W.L., Gardner, J.V., et al., *Init. Repts. DSDP,* 68: Washington (U.S. Govt. Printing Office), 455–464.

Raffi, I., and Flores, J.-A., 1995. Pleistocene through Miocene calcareous nannofossils from eastern equatorial Pacific Ocean. *In* Pisias, N.G., Mayer, L.A., Janecek, T.R., Palmer-Julson, A., and van Andel, T.H. (Eds.), *Proc. ODP, Sci. Results,* 138: College Station, TX (Ocean Drilling Program), 233–286.

Rider, M., 1996. *The Geological Interpretation of Well Logs* (2nd ed.): Caithness (Whittles Publishing).

Ruddiman, W.F., Cameron, D., and Clement, B.M., 1987. Sediment disturbance and correlation of offset holes drilled with the hydraulic piston corer: Leg 94. *In* Ruddiman, W.F., Kidd, R.B., Thomas, E., et al., *Init. Repts. DSDP,* 94 (Pt. 2): Washington (U.S. Govt. Printing Office), 615–634.

Schlumberger, 1989. *Log Interpretation Principles/Applications:* Houston, TX (Schlumberger Educ. Services).

————, 1994a. *Geological High-Resolution Magnetic Tool (GHMT) Interpretation Method:* (Schlumberger Riboud Product Center).

————, 1994b. *IPL Integrated Porosity Lithology* (Schlumberger Wireline and Testing), SMP-9270.

————, 1995. *DSI—Dipole Sonic Imager:* (Schlumberger Wireline and Testing), SMP-5128.

Schönfeld, J., 1996. The "*Stilostomella* Extinction": structure and dynamics of the last turnover in deep-sea benthic foraminiferal assemblages. *In* Mogurlevsky, A., and Whatly, R. (Eds.), *Microfossils and Oceanic Environments:* Aberystwth (Univ. Wales, Aberystwth Press), 27–37.

Serra, O., 1984. *Fundamentals of Well-Log Interpretation* (Vol. 1): *The Acquisition of Logging Data:* Dev. Pet. Sci., 15A: Amsterdam (Elsevier).

————, 1986. *Fundamentals of Well-Log Interpretation* (Vol. 2): *The Interpretation of Logging Data*. Dev. Pet. Sci., 15B.

————, 1989. *Formation MicroScanner Image Interpretation:* Houston (Schlumberger Educ. Services), SMP-7028.

Shepard, F., 1954. Nomenclature based on sand-silt-clay ratios. *J. Sediment. Petrol.,* 24:151–158.

Shipboard Scientific Party, 1995. Explanatory notes. *In* Shipley, T.H., Ogawa, Y., Blum, P., et al., *Proc. ODP, Init. Repts.,* 156: College Station, TX (Ocean Drilling Program), 39–68.

————, 1997. Explanatory notes. *In* Sigurdsson, H., Leckie, R.M., Acton, G.D., et al., *Proc. ODP, Init. Repts.,* 165: College Station, TX (Ocean Drilling Program), 15–46.

South China Sea Branch of Petroleum Corporation of the People's Republic of China, China National Geological Exploration Corporation Guangzhou Branch, Nanjing Institute of Geology and Palaeontology, Academica Sinica, Institute of Botany, Academica Sinica, Tong-Ji University, and China Academy of Geological Sciences, 1981. *Tertiary Palaeontology of North Continental Shelf of South China Sea:* Guangdong (Science and Technology Press). (in Chinese)

Stein, R., Brass, G., Graham, D., Pimmel, A., and the Shipboard Scientific Party, 1995. Hydrocarbon measurements at Arctic Gateways sites (ODP Leg 151). *In* Myhre, A.M., Thiede, J., Firth, J.V., et al., *Proc. ODP, Init. Repts.,* 151: College Station, TX (Ocean Drilling Program), 385–395.

Su, X., 1996. Development of Late Tertiary and Quaternary coccolith assemblages in the Northeast Atlantic. *GEOMAR Rep.,* 48.

Thompson, P.R., Bé, A.W.H., Duplessy, J.-C., and Shackleton, N.J., 1979. Disappearance of pink-pigmented *Globigerinoides ruber* at 120,000 yr BP in the Indian and Pacific oceans. *Nature,* 280:554–558.

Timur, A., and Toksöz, M.N., 1985. Downhole geophysical logging. *Annu. Rev. Earth Planet. Sci.,* 13:315–344.

Von Herzen, R.P., and Maxwell, A.E., 1959. The measurement of thermal conductivity of deep-sea sediments by a needle-probe method. *J. Geophys. Res.,* 64:1557–1563.

Wentworth, C.K., 1922. A scale of grade and class terms of clastic sediments. *J. Geol.,* 30:377–392.

Wyllie, M.R.J., Gregory, A.R., and Gardner, L.W., 1956. Elastic wave velocities in heterogeneous and porous media. *Geophysics,* 21:41–70.

Young, J.R., 1990. Size variation of Neogene *Reticulofenestra* coccoliths from Indian Ocean DSDP cores. *J. Micropaleontol.,* 9:71–85.

Figure F1. Schematic illustrating the possibility of changing the position of sediment (gray shading) between voids during the wire-splitting process. Note that the ash layer (black band) at 100.9 mcd in the left column (before splitting) is moved upsection because of compression/closing of voids (right column, after splitting).

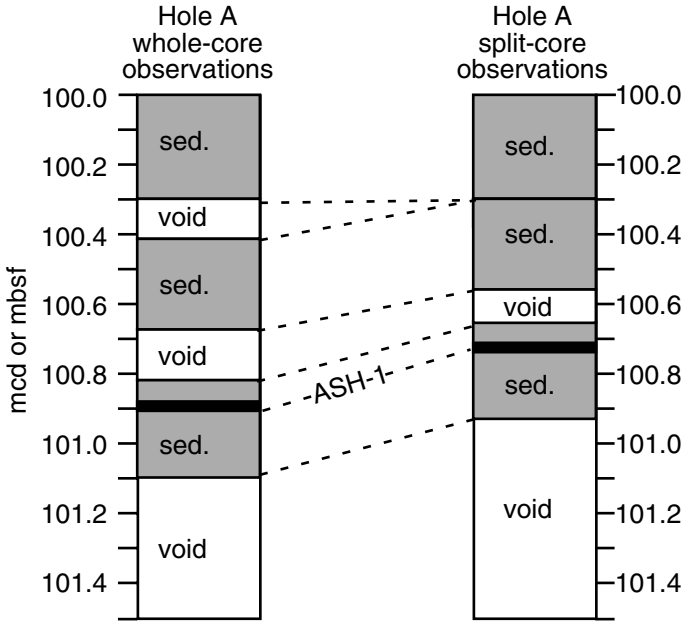

Figure F2. A. An example of a core description form. (Continued on next page.)

A

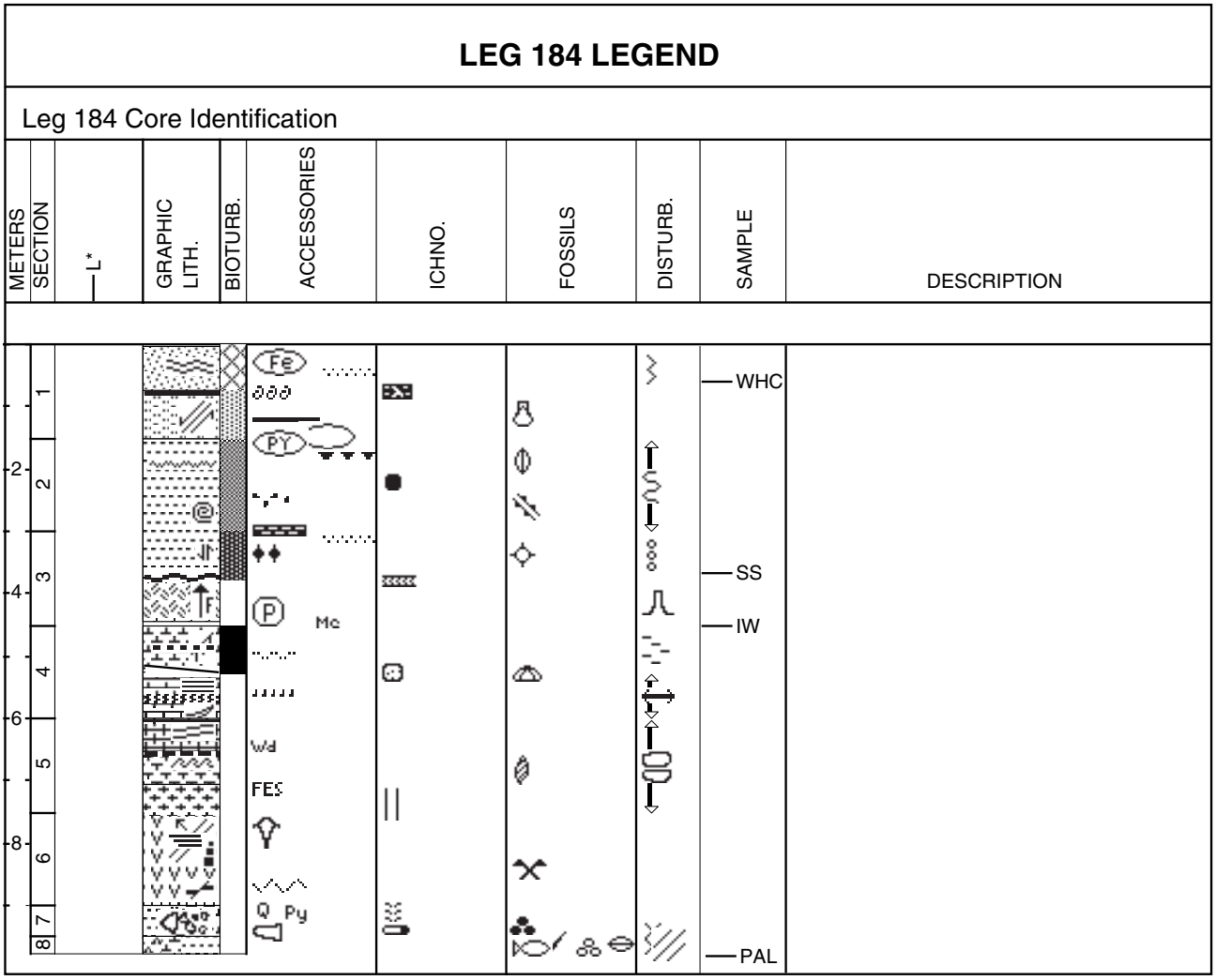

Figure F2 (continued). B. Core description legend for all sites from Leg 184.

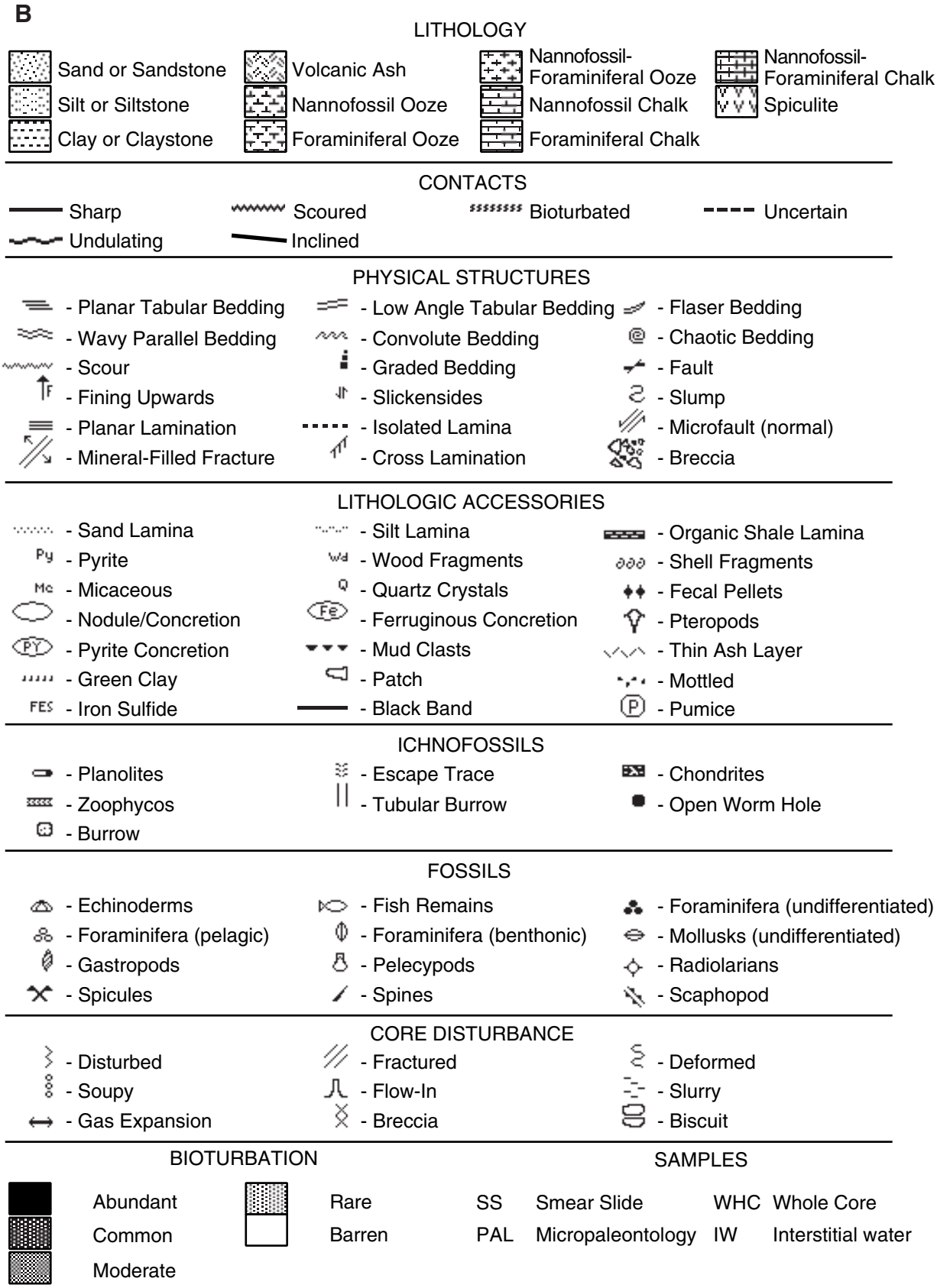

Figure F3. Udden-Wentworth grain-size classification of terrigenous sediments (from Wentworth, 1922).

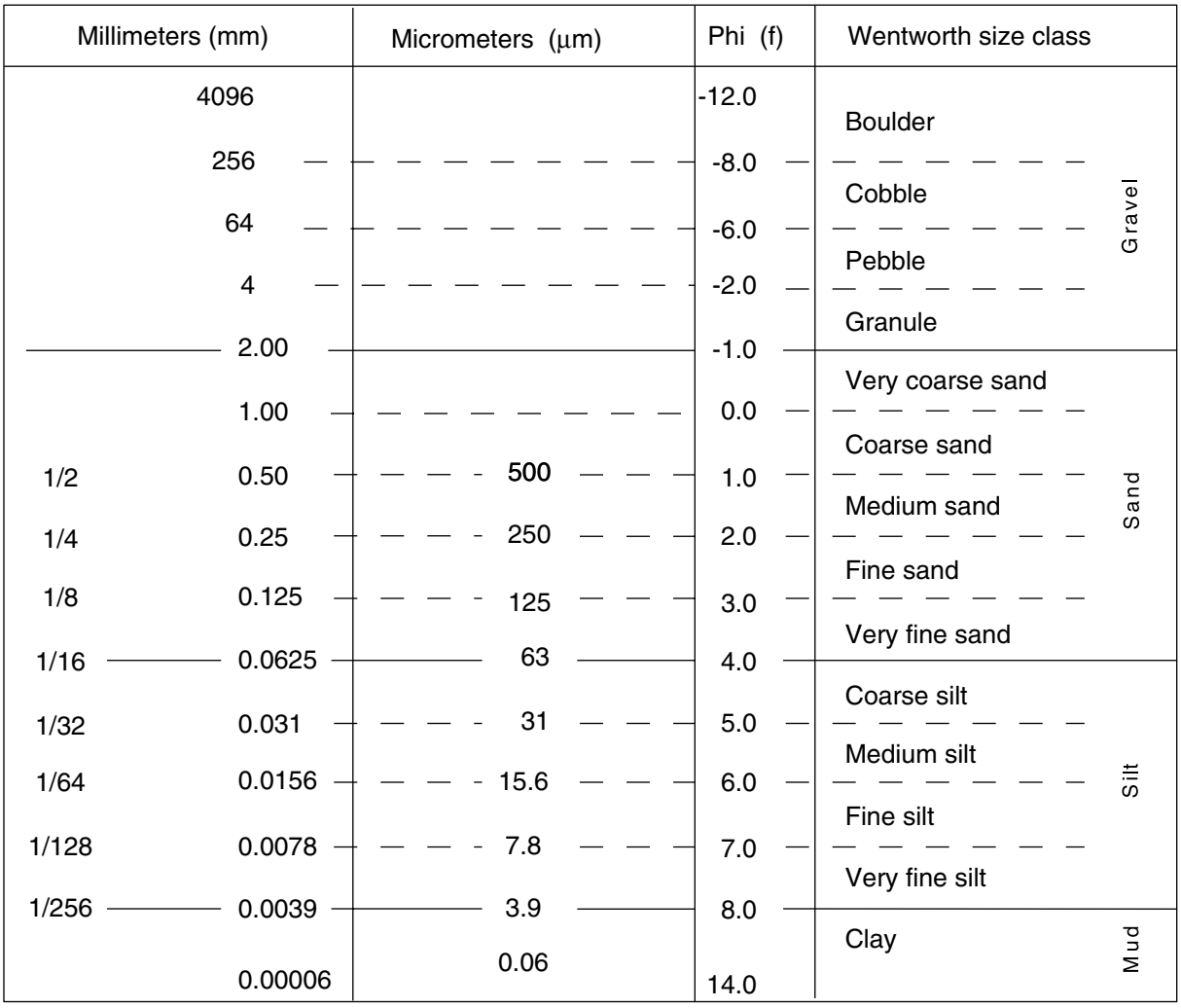

Figure F4. Diagram showing classification scheme used for siliciclastic sediments and rocks from Leg 184 (after Shepard, 1954).

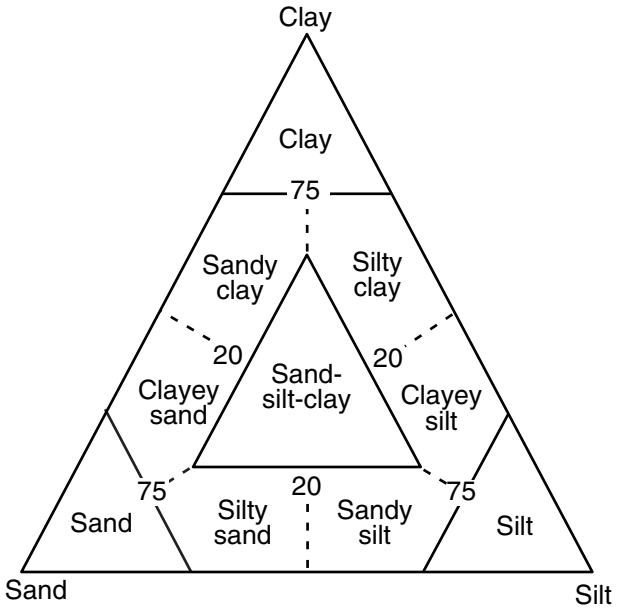

Figure F5. A. Time scale and biostratigraphic datums for the Pleistocene and Pliocene. References for calcareous nannofossil and planktonic foraminifer (underlined) datums are listed in Tables T2, p. 42, and T3, p. 43, respectively. MPTS = magnetic polarity time scale, FO = first occurrence, LO = last occurrence. (Figure adapted from Shipboard Scientific Party, 1997.) (Continued on next two pages.)

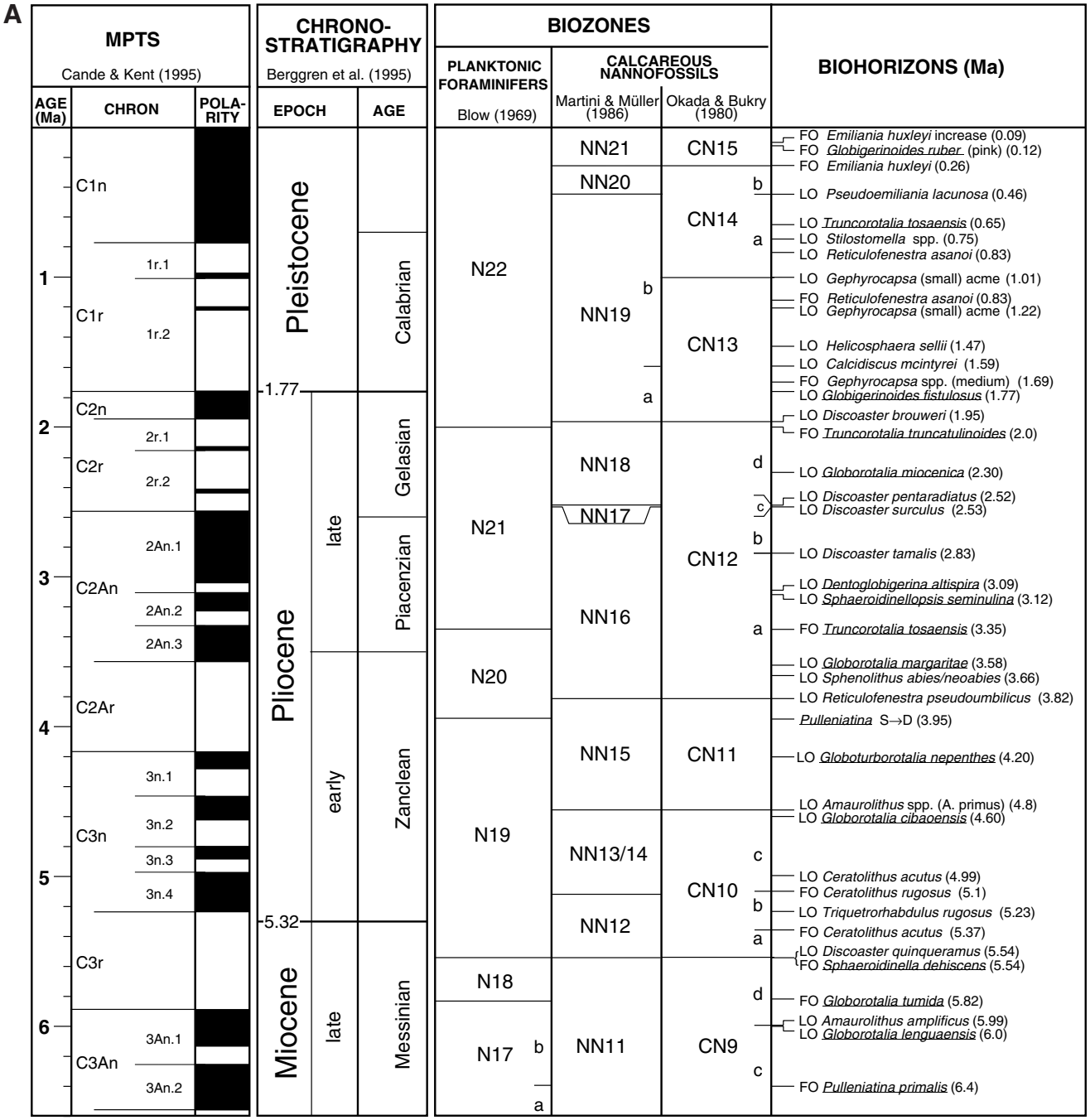

Figure F5 (continued). B. Time scale and biostratigraphic datums for the Miocene. References for calcareous nannofossil and planktonic foraminifer (underlined) datums are listed in Tables T2, p. 42, and T3, p. 43, respectively. MPTS = magnetic polarity time scale, FO = first occurrence, LO = last occurrence. (Figure adapted from Shipboard Scientific Party, 1997.)

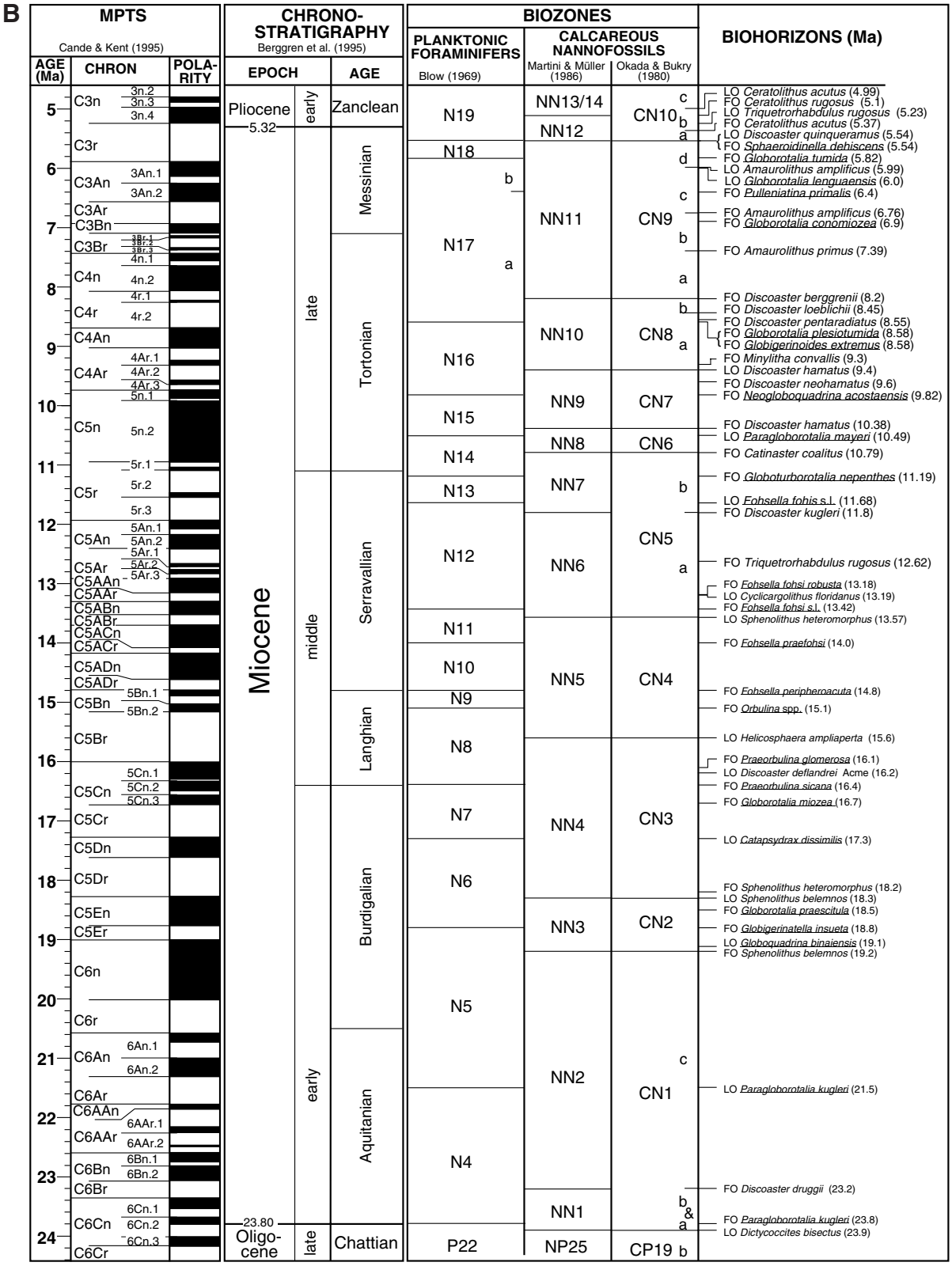

Figure F5 (continued). C. Time scale and biostratigraphic datums for the Oligocene and Eocene. References for calcareous nannofossil and planktonic foraminifer (underlined) datums are listed in Tables T2, p. 42, and T3, p. 43, respectively. MPTS = magnetic polarity time scale, FO = first occurrence, LO = last occurrence. (Figure adapted from Shipboard Scientific Party, 1997.)

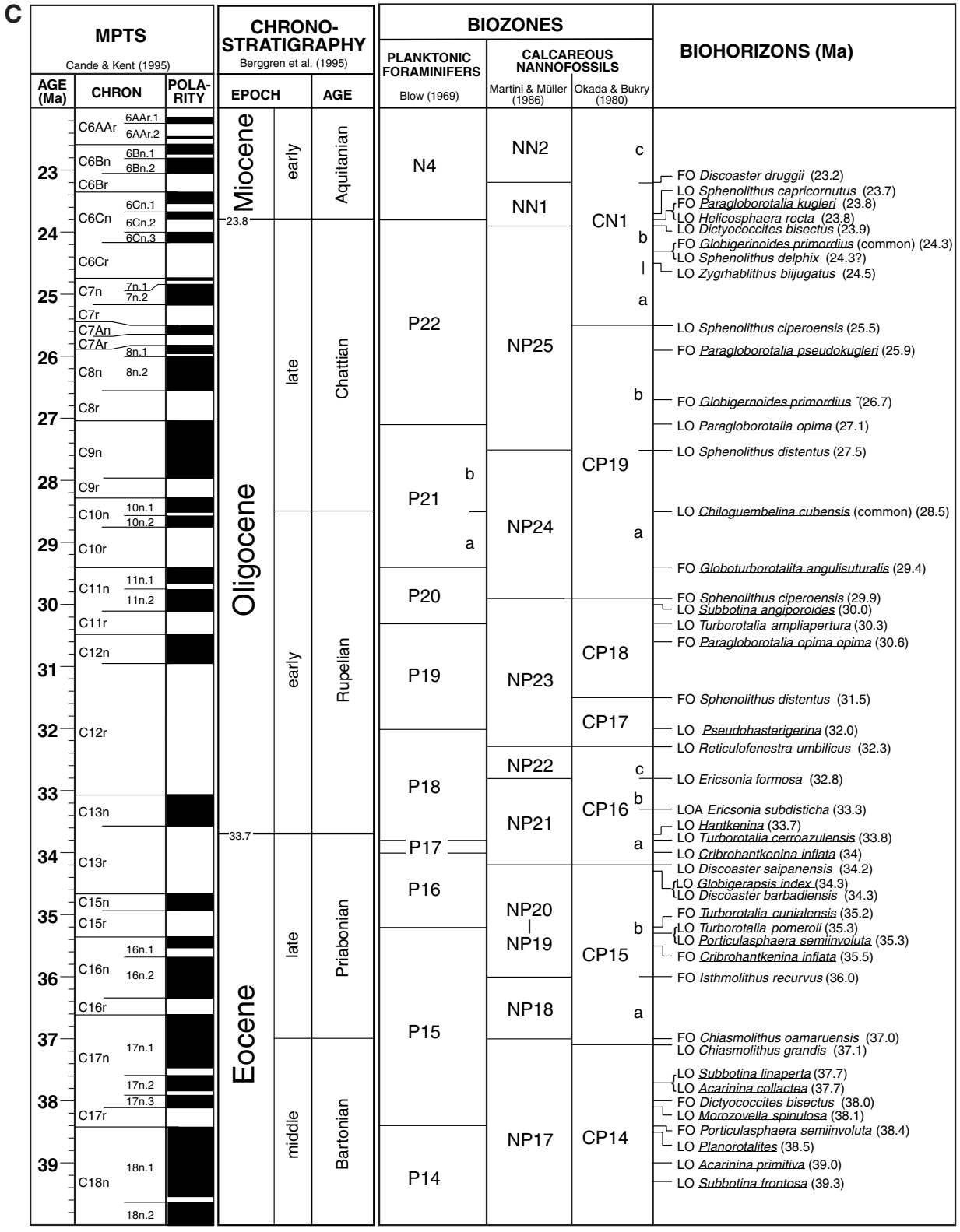

Figure F6. Schematic illustration of the configurations of tool strings run during Leg 184.

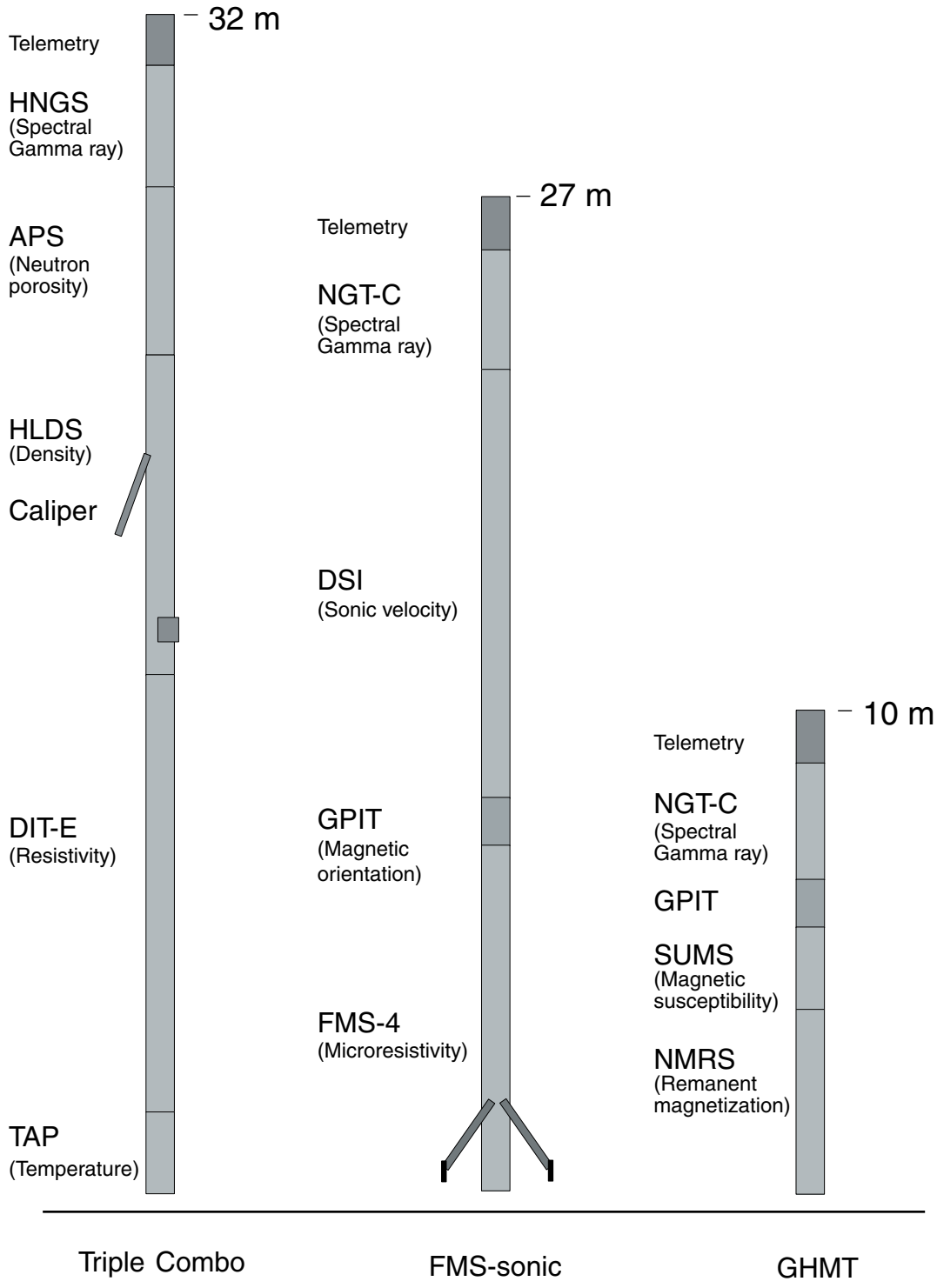

Figure F7. Schematic illustration of the DSI.

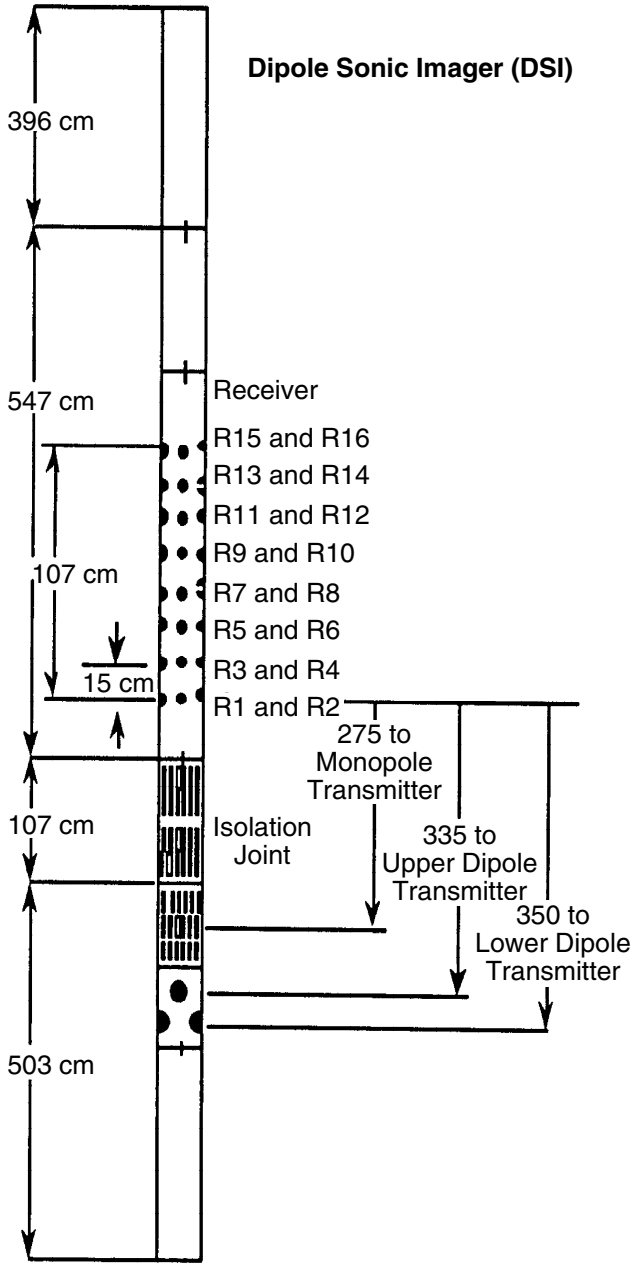

Table T1. Lithologic description of sediments and rocks, including major and minor modifiers.

Sediment class	Major modifiers	Principal names	Minor modifiers
Pelagic sediment	1. Composition of pelagic grains present in major amounts	1. Ooze	1. Composition of pelagic and neritic grains present in minor amounts
	2. Texture of clastic grains present in major amounts	2. Chalk	2. Texture of clastic grains present in minor amounts
		3. Pelagic limestone	
		4. Radiolarite	
		5. Diatomite	
		6. Spicule	
		7. Porcellanite	
		8. Chert	
Siliciclastic sediment	1. Composition of all grains present in major amounts	1. Gravel	1. Composition of all grains present in minor amounts
	2. Grain fabric (gravels only)	2. Sand	2. Texture and composition of siliciclastic grains present as matrix (for coarse-grained clastic sediments)
	3. Grain shape (optional)	3. Silt	
	4. Sediment color (optional)	4. Clay, etc.	
Volcaniclastic sediment	1. Composition of all volcaniclasts present in major amounts	1. Breccia	1. Composition of all volcaniclastics present in minor amounts
	2. Composition of all pelagic and neritic grains	2. Lapilli	2. Composition of all neritic and pelagic grains present in minor amounts
	3. Texture of siliciclastic grains present in major amounts	3. Ash/tuff	3. Texture of siliciclastic grains present in minor amounts
		4. Volcanic, etc.	

Table T2. Ages and zonations of calcareous nannofossil datum levels used during Leg 184.

Biohorizons	Zone (base)	Age (Ma)	Sources
FO *Emiliania huxleyi* acme		**0.09**	Berggren et al. (1995a)
FO *Emiliania huxleyi*	CN15/NN21	**0.26**	Berggren et al. (1995a)
LO *Pseudoemiliania lacunosa*	CN14b/NN20	**0.46**	Berggren et al. (1995a)
LO *Reticulofenestra asanoi*		**0.83**	I. Raffi (unpubl. data)
LO *Gephyrocapsa* acme (small)	CN14a	1.01	Gartner (1988); J.-P. Shyu et al. (unpubl. data)
FO *Reticulofenestra asanoi*		**1.16**	Kameo and Bralower (2000)
FO *Gephyrocapsa* acme (small)		1.22	Gartner (1988); J.-P. Shyu et al. (unpubl. data)
LO *Helicosphaera sellii*		**1.47**	Berggren et al. (1995a)
LO *Calcidiscus macintyrei*	CN13/NN19b	**1.59**	Berggren et al. (1995a)
FO *Gephyrocapsa* spp. (medium)		1.69	I. Raffi (unpubl. data)
LO *Discoaster brouweri*	CN13/NN19a	**1.95**	Berggren et al. (1995a)
LO *Discoaster pentaradiatus*	CN12d/NN18	**2.52**	I. Raffi (unpubl. data)
LO *Discoaster surculus*	CN12c/NN17	**2.53**	I. Raffi (unpubl. data)
LO *Discoaster tamalis*	CN12b	**2.83**	I. Raffi (unpubl. data)
LO *Sphenolithus abies/neoabies*		**3.66**	I. Raffi (unpubl. data); Shackleton et al. (1995)
LO *Reticulofenestra pseudoumbilicus*	CN12a/NN16	**3.82**	I. Raffi (unpubl. data)
LO *Amaurolithus* spp. (*A. primus*)	CN11a	**4.80**	Berggren et al. (1995a)
LO *Ceratolithus acutus*		**4.99**	Shackleton et al. (1995)
FO *Ceratolithus rugosus*	CN10c/NN13	**5.10**	Berggren et al. (1995a); I. Raffi (unpubl. data)
LO *Triquetrorhabdulus rugosus*		**5.23**	I. Raffi (unpubl. data)
FO *Ceratolithus acutus*	CN10b	**5.37**	I. Raffi (unpubl. data)
LO *Discoaster quinqueramus*	CN10a/NN12	**5.54**	I. Raffi (unpubl. data)
LO *Amaurolithus amplificus*		**5.99**	I. Raffi (unpubl. data)
FO *Amaurolithus amplificus*		**6.76**	I. Raffi (unpubl. data)
FO *Amaurolithus primus*	CN9b/NN11	**7.39**	I. Raffi (unpubl. data)
FO *Discoaster berggrenii*	CN9a/NN11	**8.20**	I. Raffi (unpubl. data)
FO *Discoaster loeblichii*	CN8b	8.45	Shackleton et al. (1995)
FO *Discoaster pentaradiatus*		8.55	Shackleton et al. (1995)
FO *Minylitha convallis*		9.30	Berggren et al. (1995b)
LO *Discoaster hamatus*	CN8a/NN10	9.40	Shackleton et al. (1995)
FO *Discoaster neohamatus*		9.60	Shackleton et al. (1995)
LO *Catinaster calyculus*		**9.64**	Backman and Raffi (1997)
LO *Catinaster coalitus*		**9.69**	Backman and Raffi (1997)
FO *Catinaster calyculus*	CN7b/NN9b	10.70	Berggren et al. (1995b)
FO *Discoaster hamatus*	CN7a/NN9a	10.38	Shackleton et al. (1995)
FO *Catinaster coalitus*	CN6/NN8	10.79	Shackleton et al. (1995)
LO *Discoaster kugleri*		11.52	Backman and Raffi (1997)
FO *Discoaster kugleri*	CN5b/NN7	11.83	Backman and Raffi (1997)
FO *Triquetrorhabdulus rugosus*		12.62	Shackleton et al. (1995)
LO *Cyclicargolithus floridanus*		13.19	Shackleton et al. (1995)
LO *Sphenolithus heteromorphus*	CN5a/NN6	13.57	Shackleton et al. (1995)
LO *Helicosphaera ampliaperta*	CN4/NN5	15.60	Berggren et al. (1995b)
LO *Discoaster deflandrei* acme		16.20	Shackleton et al. (1995)
FO *Sphenolithus heteromorphus*		18.20	Berggren et al. (1995b)
LO *Sphenolithus belemnos*	CN3/NN4	18.30	Berggren et al. (1995b)
FO *Sphenolithus belemnos*	CN2/NN3	19.20	Berggren et al. (1995b)
FO *Discoaster druggii*	CN1c/NN2	23.20	Berggren et al. (1995b)
LO *Sphenolithus delphix*		23.80	Berggren et al. (1995b)
LO *Dictyococcites bisectus*	CN1a, CN1b/NN1	23.90	Berggren et al. (1995b)
LO *Zygrhablithus bijugatus*		24.5	Berggren et al. (1995b)
LO *Sphenolithus ciperoensis*		25.5	Berggren et al. (1995b)
LO *Sphenolithus distentus*	CP19b/NP25	27.5	Berggren et al. (1995b)
FO *Sphenolithus ciperoensis*	CP19a/NP24	29.9	Berggren et al. (1995b)
FO *Sphenolithus distentus*	CP18	31.5	Berggren et al. (1995b)
LO *Reticulofenestra umbilicus*	CP17/NP23	32.3	Berggren et al. (1995b)
LO *Ericsonia formosa*	CP16c/NP22	32.8	Berggren et al. (1995b)
FO *Ericsonia subdisticha* acme	CP16b	33.3	Berggren et al. (1995b)
LO *Discoaster saipanensis*	CP16a/NP21	34.2	Berggren et al. (1995b)
LO *Discoaster barbadiensis*		34.3	Berggren et al. (1995b)
FO *Isthmolithus recurvus*	CP15b/NP19	36	Berggren et al. (1995b)
FO *Chiasmolithus oamaruensis*	NP18	37	Berggren et al. (1995b)
LO *Chiasmolithus grandis*	CP15a	37.1	Berggren et al. (1995b)
FO *Dictyococcites bisectus*		38	Berggren et al. (1995b)

Notes: FO = first occurrence, LO = last occurrence. The zonation codes are after Okada and Bukry (1980) and Martini and Müller (1986). Astrochronologically tuned biostratigraphic datums are depicted in bold.

Table T3. Ages and zonations of planktonic foraminifer datum levels used on Leg 184. (**See table note.** Continued on next two pages.)

Biohorizons	Zone (base)	Age (Ma)	Sources
LO *Globorotalia flexuosa*		**0.068**	Berggren et al. (1995a)
LO *Globigerinoides ruber* (pink)		**0.12**	Thompson (1979)
LO *Globoquadrina pseudofoliata*		**0.22**	Berggren et al. (1995a)
FO *Bolliella calida*		**0.22**	Berggren et al. (1995a)
FO *Globigerinoides ruber* (pink)		**0.40**	Li (1997)
FO *Globorotalia flexuosa*		**0.401**	Berggren et al. (1995a)
FO *Globorotalia hirsuta*		**0.45**	Berggren et al. (1995a)
LO *Globorotalia tosaensis*		**0.65**	Berggren et al. (1995a)
LO *Globorotalia crassiformis hessi*		**0.75**	Berggren et al. (1995a)
FO *Globorotalia truncatulinoides excelsa*		**1.00**	Berggren et al. (1995a)
LO *Globigerinoides obliquus*		**1.30**	Chaisson and Pearson (1997); Pearson and Chaisson (1997); Curry, Shackleton, Richter, et al. (1995)
LO *Pulleniatina finalis*		**1.40**	Berggren et al. (1995a)
LO *Neogloboquadrina acostaensis*		**1.58**	Chaisson and Pearson (1997); Pearson and Chaisson (1997); Curry, Shackleton, Richter, et al. (1995)
LO *Globoturborotalita apertura*		**1.64**	Berggren et al. (1995a)
LO *Globigerinoides fistulosus*		**1.77**	Berggren et al. (1995a)
LO *Globigerinoides extremus*		**1.77**	Berggren et al. (1995a)
FO *Globorotalia (Truncorotalia) truncatulinoides*	N22	**2.00**	Berggren et al. (1995a)
FO *Pulleniatina finalis*		**2.04**	Chaisson and Pearson (1997); Pearson and Chaisson (1997); Curry, Shackleton, Richter, et al. (1995)
FO *Globorotalia inflata*		**2.09**	Berggren et al. (1995a)
LO *Globorotalia (Menardella) exilis*		**2.15**	Berggren et al. (1995a)
reappearance of *Pulleniatina* (Atlantic)		**2.26**	Chaisson and Pearson (1997); Pearson and Chaisson (1997); Curry, Shackleton, Richter, et al. (1995)
LO *Globoturborotalia woodi*		**2.33**	Chaisson and Pearson (1997); Pearson and Chaisson (1997); Curry, Shackleton, Richter, et al. (1995)
LO *Globorotalia (Menardella) miocenica*		**2.30**	Berggren et al. (1995a)
LO *Globorotalia puncticulata*		**2.41**	Berggren et al. (1995a)
LO *Neogloboquadrina atlantica*		**2.41**	Berggren et al. (1995a)
LO *Globorotalia (Menardella) limbata*		**2.38**	Chaisson and Pearson (1997); Pearson and Chaisson (1997); Curry, Shackleton, Richter, et al. (1995)
LO *Globorotalia (Menardella) pertenuis*		**2.60**	Berggren et al. (1995a)
LO *Globoturborotalia decoraperta*		**2.75**	Chaisson and Pearson (1997); Pearson and Chaisson (1997); Curry, Shackleton, Richter, et al. (1995)
LO *Globorotalia (Menardella) multicamerata*		**3.09**	Berggren et al. (1995a)
LO *Dentoglobigerina altispira*		**3.09**	Berggren et al. (1995a)
LO *Sphaeroidinellopsis seminulina*		**3.12**	Berggren et al. (1995a)
LO *Globorotalia (Hirsutella) cibaoensis*		**3.22**	Chaisson and Pearson (1997); Pearson and Chaisson (1997); Curry, Shackleton, Richter, et al. (1995)
LO *Globoquadrina baroemoenensis*		**3.22**	Chaisson and Pearson (1997); Pearson and Chaisson (1997); Curry, Shackleton, Richter, et al. (1995)
FO *Sphaeroidinella dehiscens* s.s.		**3.25**	Berggren et al. (1995a)
FO *Globigerinoides fistulosus*		**3.33**	Berggren et al. (1995a)
FO *Globorotalia (Truncorotalia) tosaensis*	N21	**3.35**	Berggren et al. (1995a)
LO *Pulleniatina* (Atlantic)		**3.45**	Berggren et al. (1995a)
FO *Globorotalia (Menardella) pertenuis*		**3.45**	Berggren et al. (1995a)
LO *Globorotalia plesiotumida*		**3.77**	Chaisson and Pearson (1997); Pearson and Chaisson (1997); Curry, Shackleton, Richter, et al. (1995)
FO *Globorotalia (Menardella) miocenica*		**3.55**	Berggren et al. (1995a)
LO *Globorotalia (Hirsutella) margaritae*		**3.58**	Berggren et al. (1995a)
LO *Pulleniatina primalis*		**3.65**	Berggren et al. (1995a)
Pulleniatina (sinistral to dextral coiling change)	N20	**3.95**	Berggren et al. (1995a)
LO *Globorotalia margaritae* (common)		**3.96**	Berggren et al. (1995a)
LO *Globoturborotalita nepenthes*		**4.20**	Berggren et al. (1995a)
LO *Pulleniatina spectabilis*		**4.20**	Berggren et al. (1995a)
FO *Globorotalia (Menardella) exilis*		**4.45**	Chaisson and Pearson (1997); Pearson and Chaisson (1997); Curry, Shackleton, Richter, et al. (1995)
FO *Globorotalia puncticulata*		**4.50**	Berggren et al. (1995a)
FO *Globorotalia (Truncorotalia) crassaformis* s.l.		**4.5**	Berggren et al. (1995a)
LO *Sphaeroidinellopsis kochi*		**4.53**	Chaisson and Pearson (1997); Pearson and Chaisson (1997); Curry, Shackleton, Richter, et al. (1995)
LO *Globorotalia cibaoensis*		**4.6**	Berggren et al. (1995a)
LO *Globigerinoides seiglei*		**4.70**	Berggren et al. (1995a)
FO *Globorotalia margaritae* (common)		5.07	Berggren et al. (1995a)
LO *Globoquadrina dehiscens*		**5.49**	Shackleton et al. (1995)
FO *Sphaeroidinella dehiscens* s.l.	N19	**5.54**	Chaisson and Pearson (1997); Pearson and Chaisson (1997); Curry, Shackleton, Richter, et al. (1995)
FO *Globorotalia pliozea*		5.60	Berggren et al. (1995b)

Table T3 (continued).

Biohorizons	Zone (base)	Age (Ma)	Sources
FO *Globorotalia sphericomiozea*		5.60	Berggren et al. (1995b)
FO *Globorotalia tumida*	N18	**5.82**	Chaisson and Pearson (1997); Pearson and Chaisson (1997); Curry, Shackleton, Richter, et al. (1995)
FO *Turborotalia humilis*		**5.84**	Chaisson and Pearson (1997); Pearson and Chaisson (1997); Curry, Shackleton, Richter, et al. (1995)
LO *Globorotalia lenguaensis*		6.0	Berggren et al. (1995b)
FO *Globorotalia (Hirsutella) margaritae*		**6.09**	Chaisson and Pearson (1997); Pearson and Chaisson (1997); Curry, Shackleton, Richter, et al. (1995)
FO *Globigerinoides conglobatus*		**6.20**	Chaisson and Pearson (1997); Pearson and Chaisson (1997); Curry, Shackleton, Richter, et al. (1995)
FO *Pulleniatina primalis*	N17b	6.4	Berggren et al. (1995b)
Neogloboquad. acostaensis (dextral to sinistral coiling change)		6.6	Berggren et al. (1995b)
FO *Globorotalia conomiozea*		6.9	Berggren et al. (1995b)
FO *Candeina nitida*		**8.44**	Chaisson and Pearson (1997); Pearson and Chaisson (1997); Curry, Shackleton, Richter, et al. (1995)
FO *Neogloboquadrina humerosa*		8.5	Berggren et al. (1995b)
FO *Globigerinoides extremus*		**8.58**	Chaisson and Pearson (1997); Pearson and Chaisson (1997); Curry, Shackleton, Richter, et al. (1995)
FO *Globorotalia plesiotumida*	N17a	**8.58**	Chaisson and Pearson (1997); Pearson and Chaisson (1997); Curry, Shackleton, Richter, et al. (1995)
FO *Globorotalia (Hirsutella) cibaoensis*		**9.44**	Chaisson and Pearson (1997); Pearson and Chaisson (1997); Curry, Shackleton, Richter, et al. (1995)
FO *Globorotalia (Hirsutella) juanai*		**9.76**	Chaisson and Pearson (1997); Pearson and Chaisson (1997); Curry, Shackleton, Richter, et al. (1995)
FO *Neogloboquadrina acostaensis*	N16	**9.82**	Chaisson and Pearson (1997); Pearson and Chaisson (1997); Curry, Shackleton, Richter, et al. (1995)
LO *Neogloboquadrina nympha*		10.1	Berggren et al. (1995b)
LO *Paragloborotalia mayeri*	N15	**10.49**	Chaisson and Pearson (1997); Pearson and Chaisson (1997); Curry, Shackleton, Richter, et al. (1995)
FO *Globorotalia (Menardella) limbata*		**10.57**	Chaisson and Pearson (1997); Pearson and Chaisson (1997); Curry, Shackleton, Richter, et al. (1995)
FO *Globoturborotalita apertura*		**11.19**	Chaisson and Pearson (1997); Pearson and Chaisson (1997); Curry, Shackleton, Richter, et al. (1995)
FO *Globoturborotalita decoraperta*		**11.46**	Chaisson and Pearson (1997); Pearson and Chaisson (1997); Curry, Shackleton, Richter, et al. (1995)
FO *Sphaeroidinellopsis subdehiscens*		11.74	Shackleton et al. (1995)
FO *Globoturborotalita nepenthes*	N14	**11.19**	Chaisson and Pearson (1997); Pearson and Chaisson (1997); Curry, Shackleton, Richter, et al. (1995)
LO *Globorotalia panda*		11.8	Berggren et al. (1995b)
LO *Globorotalia praescitula*		11.9	Berggren et al. (1995b)
LO *Fohsella fohsi* s.l. (including *fohsi lobata* and *fohsi robusta*)	N13	**11.68**	Chaisson and Pearson (1997); Pearson and Chaisson (1997); Curry, Shackleton, Richter, et al. (1995)
FO *Globorotalia lenguaensis*		**12.85**	Chaisson and Pearson (1997); Pearson and Chaisson (1997); Curry, Shackleton, Richter, et al. (1995)
FO *Fohsella fohsi robusta*		**13.18**	Chaisson and Pearson (1997); Pearson and Chaisson (1997); Curry, Shackleton, Richter, et al. (1995)
FO *Fohsella fohsi* s.l.	N12	**13.42**	Chaisson and Pearson (1997); Pearson and Chaisson (1997); Curry, Shackleton, Richter, et al. (1995)
FO *Fohsella praefohsi*	N11	14.0	Chaisson and Pearson (1997)
FO *Neogloboquadrina nympha*		13.4	Berggren et al. (1995b)
LO *Clavatorella bermudezi*		14.2	Chaisson and Pearson (1997); Pearson and Chaisson (1997); Curry, Shackleton, Richter, et al. (1995)
LO *Globorotalia archeomenardii*		14.2	Chaisson and Pearson (1997); Pearson and Chaisson (1997); Curry, Shackleton, Richter, et al. (1995)
LO *Fohsella peripheroronda*		14.6	Berggren et al. (1995b)
FO *Fohsella peripheroacuta*	N10	14.8	Berggren et al. (1995b)
LO *Praeorbulina sicana*		14.8	Berggren et al. (1995b)
LO *Praeorbulina glomerosa*		14.8	Berggren et al. (1995b)
FO *Globorotalia (Menardella) praemenardii*		14.9	Chaisson and Pearson (1997); Pearson and Chaisson (1997); Curry, Shackleton, Richter, et al. (1995)
LO *Globigerinatella insueta*		15.0	Chaisson and Pearson (1997); Pearson and Chaisson (1997); Curry, Shackleton, Richter, et al. (1995)
FO *Orbulina* spp.	N9	15.1	Berggren et al. (1995b)
FO *Globorotalia (Menardella) archeomenardii*		15.5	Chaisson and Pearson (1997); Pearson and Chaisson (1997); Curry, Shackleton, Richter, et al. (1995)
FO *Clavatorella bermudezi*		15.8	Chaisson and Pearson (1997); Pearson and Chaisson (1997); Curry, Shackleton, Richter, et al. (1995)
LO *Globorotalia miozea*		15.9	Berggren et al. (1995b)
FO *Praeorbulina circularis*		16.0	Berggren et al. (1995b)
FO *Praeorbulina glomerosa*		16.10	Berggren et al. (1995b)
FO *Globigerinoides diminutus*		16.1	Berggren et al. (1995b)
FO *Praeorbulina curva*		16.3	Berggren et al. (1995b)
FO *Praeorbulina sicana*	N8	16.4	Berggren et al. (1995b)
LO *Globorotalia incognita*		16.4	Berggren et al. (1995b)

Table T3 (continued).

Biohorizons	Zone (base)	Age (Ma)	Sources
FO *Globorotalia miozea*		16.7	Berggren et al. (1995b)
FO *Globorotalia birnageae*		16.7	Berggren et al. (1995b)
LO *Catapsydrax dissimilis*	N7	17.3	Berggren et al. (1995b)
LO *Globorotalia zealandica*		17.3	Berggren et al. (1995b)
LO *Globorotalia semivera*		17.3	Berggren et al. (1995b)
FO *Globorotalia praescitula*		18.5	Berggren et al. (1995b)
FO *Globigerinatella insueta*	N6	18.8	Berggren et al. (1995b)
LO *Globoquadrina binaiensis*		19.1	Chaisson and Pearson (1997); Pearson and Chaisson (1997); Curry, Shackleton, Richter, et al. (1995)
FO *Globigerinoides altiapertura*		20.5	Berggren et al. (1995b)
LO *Tenuitella munda*		21.4	Berggren et al. (1995b)
LO *Paragloborotalia kugleri*	N5	21.5	Berggren et al. (1995b)
FO *Globorotalia incognita*		21.6	Berggren et al. (1995b)
LO *Globoturborotalita angulisuturalis*		21.6	Berggren et al. (1995b)
LO *Paragloborotalia pseudokugleri*		21.6	Berggren et al. (1995b)
FO *Globoquadrina binaiensis*		22.1	Berggren et al. (1995b)
FO *Globoquadrina dehiscens*		23.2	Berggren et al. (1995b)
LO *Globigerina ciperoensis*		23.3	Chaisson and Pearson (1997); Pearson and Chaisson (1997); Curry, Shackleton, Richter, et al. (1995)
FO *Globigerinoides trilobus* s.l.		23.4	Chaisson and Pearson (1997); Pearson and Chaisson (1997); Curry, Shackleton, Richter, et al. (1995)
FO *Paragloborotalia kugleri*	N4	23.8	Berggren et al. (1995b)
LO *Globigerina euapertura*		23.8	Berggren et al. (1995b)
FO *Globigerinoides primordius* (common)		24.3	Berggren et al. (1995b)
LO *Tenuitella gemma*		24.3	Berggren et al. (1995b)
FO *Paragloborotalia pseudokugleri*		25.9	Berggren et al. (1995b)
FO *Globigerinoides primordius*		26.7	Berggren et al. (1995b)
LO *Paragloborotalia opima*	P22	27.1	Berggren et al. (1995b)
LO *Globigerina labiacrassata*		27.1	Berggren et al. (1995b)
LO *Chiloguembelina cubensis* (common)	P21b	28.5	Berggren et al. (1995b)
FO *Globoturborotalita angulisuturalis*	P21a	29.4	Berggren et al. (1995b)
LO *Subbotina angiporoides*		30.0	Berggren et al. (1995b)
LO *Turborotalia ampliapertura*	P20	30.3	Berggren et al. (1995b)
FO *Paragloborotalia opima*		30.6	Berggren et al. (1995b)
LO *Pseudohastigerina* spp.	P19	32.0	Berggren et al. (1995b)
FO *Cassigerinella chipolensis*		33.65	Berggren et al. (1995b)
LO *Hantkenina* spp.		33.7	Berggren et al. (1995b)
LO *Turborotalia cerroazulensis*	P18	33.8	Berggren et al. (1995b)
LO *Cribrohantkenina inflata*	P17	34.0	Berggren et al. (1995b)
LO *Clavigerinella eocanica*		34.0	Chaisson and Pearson (1997); Pearson and Chaisson (1997); Curry, Shackleton, Richter, et al. (1995)
LO *Globogerapsis index*		34.3	Berggren et al. (1995b)
FO *Turborotalia cunialensis*	P16	35.2	Berggren et al. (1995b)
LO *Turborotalia pomeroli*		35.3	Berggren et al. (1995b)
LO *Porticulasphaera semiinvoluta*		35.3	Berggren et al. (1995b)
FO *Cribrohantkenina inflata*		35.5	Berggren et al. (1995b)
LO *Acarinina collactea*		37.7	Berggren et al. (1995b)
LO *Subbotina linaperta*		37.7	Berggren et al. (1995b)

Notes: LO = last occurrence, FO = first occurrence. The zonation codes are after Blow (1969). Astrochronologically tuned biostratigraphic datums are depicted in bold.

Table T4. Logging tool and measurement acronyms and units of measurement.

Tool	Output	Explanation	Units
HNGS		Hostile environment natural gamma-ray sonde	
	HSGR	Standard (total) gamma ray	gAPI
	HCGR	Computed gamma-ray (HSGR – uranium contribution)	gAPI
	HFK	Formation potassium	wt%
	HTHO	Thorium	ppmv
	HURA	Uranium	ppmv
NGT		Natural gamma-ray tool	
	SGR	Standard total gamma ray	gAPI
	CGR	Computed gamma-ray (SGR – uranium contribution)	gAPI
	POTA	Potassium	wt%
	THOR	Thorium	ppmv
	URAN	Uranium	ppmv
APS		Accelerator porosity sonde	
	APLC	Near array porosity (limestone corrected)	Fraction
	FPLC	Far array porosity (limestone corrected)	Fraction
	SIGF	Neutron capture cross section of the formation (Sf)	c. units
	STOF	Tool standoff (computed distance from borehole wall)	in
HLDS		Hostile environment lithodensity sonde	
	RHOM	Bulk density (corrected)	g/cm^3
	PEF	Photoelectric effect	$barn/e^-$
	LCAL	Caliper-measure of borehole diameter	in
	DRH	Bulk density correction	g/cm^3
DITE-SFL		Dual induction tool–spherically focused log	
	IDPH	Deep induction phasor-processed resistivity	Wm
	IMPH	Medium induction phasor-processed resistivity	Wm
	SFLU	Shallow spherically focused resistivity	Wm
GHMT		Geological high-resolution magnetic tool	
	MAGS	Magnetic susceptibility (limited range)	IU
	RMGS	Low resolution magnetic susceptibility (wider range)	IU
	MAGC	Earth conductivity	IU
	MAGB	Earth total magnetic field	nT
DSI		Dipole sonic imager	
	DT 1S	Shear slowness	ms/f
	DT 2S	Shear slowness	ms/f
	DT 4P	Compressional slowness	ms/f
FMS		Formation MicroScanner	
	C1, C2	Caliper	cm
LDEO-TAP		Lamont-Doherty temperature/acceleration/pressure tool	°C, mm/s^2, psi
GPIT		General-purpose inclinometer tool	
	DEVI	Hole deviation from vertical	°
	HAZI	Azimuth of deviation	°

Notes: gAPI = American Petroleum Institute unit of measurement for gamma ray. IU = instrument units.

Table T5. Specifications of the logging tools used during Leg 184 grouped into tool strings.

Tool strings	Typical logging speed (m/hr)	Individual tools	Properties measured	Sample interval (cm)	Approximate vertical resolution (cm)	Approximate depth of investigation (cm)
Triple combination (total length = ~32 m)	250-275	HNGS	Natural gamma ray	15	55	Variable
		APS	Porosity	5 and 15	30	15
		HLDS	Bulk density, photoelectric effect	15	38	15
		DITE-SFL	Resistivity	15	200/150/90/60	150/76/38
		TAP	Temperature, acceleration, pressure	1 per s, 4 per s, 1 per s	NA	NA
FMS-sonic (total length = ~30 m)	500-550	NGT	Natural gamma ray	15	55	46
		DSI	Sonic velocity	15	110	15-30
		GPIT	Tool orientation	1 or 15	NA	NA
		FMS	Resistivity image	0.25	0.5	15
GHMT (total length = ~10 m)	300-400	NGT	Natural gamma ray	15	55	25
		SUMS	Susceptibility	5 and 15	35	NA
		NMRS	Total field	15	45	NA

Notes: See Table **T4**, p. 46, for explanations of acronyms used to describe tool strings and individual tool names. NA = not applicable.

Table T6. LDEO-TAP tool specifications (memory mode).

Specification	Measurement
Acceleration measurement range	–2 G to +2 G
Acceleration resolution	1 mm/s^2
Acceleration sampling rate:	
LR mode	4 Hz
HR mode	8 Hz
Temperature measurement range	–4°C to +85°C
Temperature resolution	0.005°C
Pressure measurement range	0 to 10, 000 psi
Pressure resolution	1 psi
Pressure measurement precision	0.1% FS
Temperature/pressure sampling rate	1 Hz
Total data recording time:	
HR mode	5 hr
LR mode	8 hr
Power source	8 alkaline batteries (D type)
Total operation time off one set of batteries	~40 hr

Notes: HR = high resolution, LR = low resolution. LDEO = Lamont-Doherty Earth Observatory, TAP = temperature/acceleration/pressure.